Shadow Cast by Black Holes under the Influence of Plasma and Shadow Geometry of Naked Singularities

By

Saira Yasmin

(Registration No: 403070)

A thesis submitted to the National University of Sciences and Technology, Islamabad,

in partial fulfillment of the requirements for the degree of

Master of Science in

Mathematics

Supervisor: Dr. Mubasher Jamil

Department of Mathematics,

School of Natural Sciences,

National University of Sciences and Technology (NUST),

Islamabad, Pakistan (2024).

THESIS ACCEPTANCE CERTIFICATE

Certified that final copy of MS thesis written by **Saira Yasmin** (Registration No **00000403070**), of **School of Natural Sciences** has been vetted by undersigned, found complete in all respects as per NUST statutes/regulations, is free of plagiarism, errors, and mistakes and is accepted as partial fulfillment for award of MS/M.Phil degree. It is further certified that necessary amendments as pointed out by GEC members and external examiner of the scholar have also been incorporated in the said thesis.

Signature: _____

Name of Supervisor: Prof. Mubasher Jamil

Date: _____

Signature (HoD): _____

Date: 05-11-2024
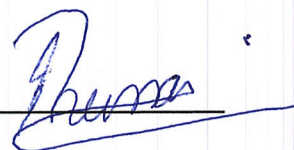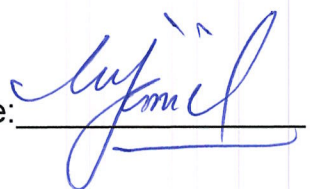
Signature (Dean/Principal): _____

Date: 06.11.2024

National University of Sciences & Technology

MS THESIS WORK

We hereby recommend that the dissertation prepared under our supervision by: <u>Saira Yasmin,</u> Regn No. <u>00000403070,</u> Titled <u>Shadow Cast by Black Holes under the Influence of Plasma and Shadow Geometry of Naked Singularities</u> be Accepted in partial fulfillment of the requirements for the award of MS degree.

Examination Committee Members

1. Name: <u>PROF. MERAJ MUSTAFA HASHMI</u>　　　　Signature: _____

2. Name: <u>PROF. IBRAR HUSSAIN</u>　　　　　　　　　Signature: _____

Supervisor's Name <u>PROF. MUBASHER JAMIL</u>　　　　Signature: _____

_____　　　　　　　　　5－11－2024
Head of Department　　　　　　　　　　　　　　　Date

COUNTERSINGED

Date: 06. 11.2024　　　　　　　　　　_____
　　　　　　　　　　　　　　　　　　　　　Dean/Principal

Dedicated

to

Allah Almighty and My Parents

ACKNOWLEDGEMENT

Contents

III

List of Tables

List of Figures

VII

VII

VIII

IX

LIST OF ABBREVIATIONS

GTR   General Theory of Relativity

EHT   Event Horizon Telescope

CCC   Cosmic Censorship Conjecture

MOG   Modified Gravity

KNSs   Kerr Naked Singularities

DM   Dark Matter

KMNSs   Kerr MOG Naked Singularities

SMBHs   Supermassive Black Holes

STVG   Scalar Tensor Vector Gravity

HJ   Hamilton Jacobi

Abstract

The investigation of black holes and naked singularity shadows has attracted much attention in modern astrophysics research. The shadow of black holes in the presence of plasma and naked singularities will be computed in this dissertation. We will observe the propagation of light in a non-magnetized plasma around a Kerr and Ker MOG black hole. Particularly, we formulate an analytical formula for the boundary curves of shadow on the observer's sky, regardless of where they are in the outer communication domain. The shadow's shape and size that is observed varies based on plasma properties. Recently the Event Horizon Telescope's direct imaging of supermassive black holes (SMBHs) at the event horizon scaling factors, allows for testing alternative models to supermassive black holes such as Kerr naked singularities (KNSs) and Kerr MOG naked singularities (KMNSs). The shadow of KNSs and KMNSs can be utilized to assess the cosmic censorship theory, and KNSs and KMNSs can be used as substitute models for SMBHs by comparing them with black hole shadow measurements.

Chapter 1

Introduction

In 1783, the idea of *Black Holes* was first presented by the English natural philosopher John Michell [1]. The black holes are regions of spacetime from which nothing can evade their gravitational pulling even light. He calculated the imperative radius for the star to be dense like the sun so that its powerful gravity prevents any light from escaping. For example, the star's surface escape velocity has to exceed the speed of light. He mentioned that, these stars as dark stars because the emission of light beams at the surface cannot escape them. After that, Laplace [1] discussed the same concept of a star bigger than the sun and absorbing light beams from all around it. These initiatives were all based on Newton's theory of gravity and light. Therefore, they presented that light cannot escape these stars due to the immense gravity they have.

In 1915, Einstein established his General Theory of Relativity (GTR) [2], which is entirely distinct from the description of gravity presented by Newton. Newton described gravity as a force acting between two masses over a distance. However, Einstein's General Theory of Relativity (GTR) redefines gravity as the curvature of spacetime, influenced by mass. Massive bodies such as the Earth and the Sun distort spacetime, and this curvature influences the paths that objects follow. The GTR of Einstein gave counter-intuitive and amazing consequences. In particular, the problem of the orbit of Mercury was resolved[3]. In this problem, the precession of the perihelion of Mercury was observed to be different

from the predictions of Newton's theory of gravity. Although the difference was not big, Newton's theory failed to explain it, while GTR was reliable with the observations. Besides, one inordinate consequence of GTR is black holes. However, Michell's black holes (dark stars) are changed from the GTR black holes meaning that the latter do not need to possess very powerful gravity. The main idea depends on the nature of the black hole geodesics. A generalization of the straight line in Euclidean space is geodesic. So, geodesic is the shortest straight path between two points on curved spacetime. Hence the time taken by a particle must be minimized to travel between two points in this space. Black holes in GTR usually consist of the following; the black hole event horizon, which is the boundary of the black hole, and a singularity, which means a space-like point where all the mass of the black hole is centralized, and nothing will be able to escape the black hole if it passes it. Moreover, in 1960s, Hawking and Penrose developed theorems about black holes, like black hole thermodynamics [4]. For example, Hawking's area theorem which is the second law of black hole thermodynamics describes that the rate of change of the area of the event horizon of a black hole cannot decrease [5]. This is similar to the second law of thermodynamics which the entropy change is nondecreasing.

The first mathematical exact solution to Einstein's theory of gravitation was developed by Karl Schwarzschild, a German astronomer and physicist, in 1916. This solution, known as the Schwarzschild solution [6], was originally intended to describe the gravitational field around a spherical star. However, when considered as a general solution without the presence of a star, a critical radius now known as the Schwarzschild or gravitational radius emerges. This radius is much smaller than the star's radius and does not factor into solutions that include a central star. Furthermore, the properties of the region enclosed by this radius are unusual, leading to its dismissal for many years as irrelevant to astrophysics, especially since it was difficult to interpret physically. So, after this, notable advancements in both theoretical and observational studies were noted. In 1963, physicist Roy Kerr from the University of Austin, Texas, found the exact solution for a rotating vacuum object in the framework of general relativity [7]. By setting the rotation

parameter to zero in the Kerr solution, one can recover the Schwarzschild solution. The significance of both the Schwarzschild and Kerr solutions in the fields of physics and astrophysics was so profound that they warranted specific names. In 1968, a publication by John Archibald Wheeler coined the term 'black holes' to describe these objects [8]. As a result, the vacuum solutions of Schwarzschild and Kerr came to be known as Schwarzschild and Kerr black holes, respectively.

1.1   Observational Insights into Black Holes

The problem with Newtonian gravitational theory is that it does not work when we have a strong gravitational field, such as near the sun, consequently, Newton's theory failed to match the observational data about the orbit of Mercury near the sun. However, it confirms that GTR works quite well, we have to test it in a strong gravitational field, such as in the vicinity of a black hole. It means that by testing we have to use the theory to expect things about black holes, and subsequently try to match the theoretical findings with observations. From the GTR calculations, we can find that our universe is capable of having black holes [5]. However, this does not say whether we have black holes in our universe, an observation is needed. There are two ways to observe an object in the sky. An object either emits light directly toward human eyes or telescopes, or it emits light that is reflected until it eventually reaches the observer. Black holes are unable to be observed directly because light emitted toward them is absorbed by them. Rather, astrophysicists used indirect observational methods like examining the gravitational effect of black holes on the light beams or generally electromagnetic waves that move near them. In [9], the authors inferred the existence of a black hole because of the electromagnetic wave bending effect. Other black holes, such as supermassive and stellar-mass black holes were also discovered using similar methods. And the notable examples of stellar-mass black hole candidates, such as Cygnus X-1 and LMC X-3. These systems have been instrumental in confirming the presence of stellar-mass black holes, as

their influence on surrounding stars and radiation from accretion processes offer significant observational evidence. In April 2019, an international collaboration of scientists Event Horizon Telescope (EHT Collaboration) revealed an image showing an asymmetric blurred ring around a dark shadow [10].

After comparison with computer models, the picture was interpreted as showing a supermassive black hole at the center of the galaxy Messier 87* (M87*) [11]. This interpretation fits well with theory and simulation, according to which the M87* black hole is one of the two largest supermassive black holes in the sky along with the Sagittarius A* (Sgr A*) black hole (at the center of the Milky Way, near the border of the constellations Sagittarius and Scorpius) [12] and we can see these in Fig. (1.1) [13].
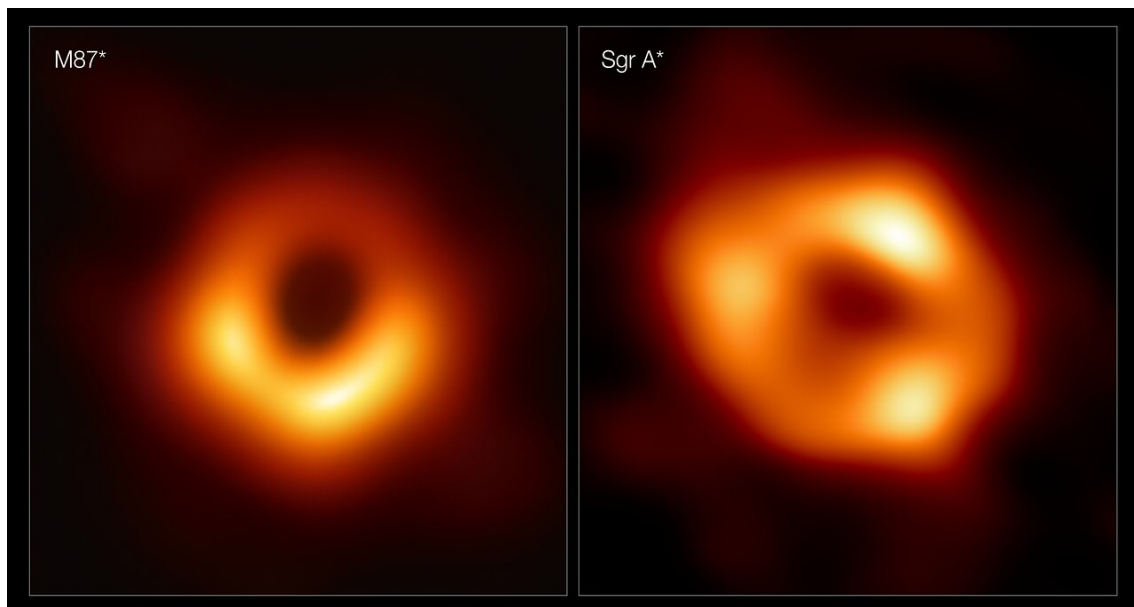
Figure 1.1. The images in these panels represent the first successful captures of black holes. The left panel shows M87*, the massive black hole situated in the center of the M87*, located 55 million light-years from Earth. The right panel features Sagittarius A* (Sgr A*), positioned at the core of our Milky Way. Despite M87* being roughly a thousand times larger than Sgr A*, both appear similarly sized in the images. These visuals were produced using the Event Horizon Telescope (EHT), a worldwide network of radio telescopes. This network includes the Atacama Large Millimeter/submillimeter Array (ALMA) and the Atacama Pathfinder EXperiment (APEX), in which the European Southern Observatory (ESO) is a partner.

1.2   Shadow of Black Holes

The shadow of a black hole describes the dark region in space surrounding the event horizon, which is the boundary beyond which nothing can escape the gravitational pull of the black hole, not even light. When a black hole is positioned between a luminous background source and an observer, its gravitational field functions as a lens, causing the light from the source to bend. If the observer aligns with the path of the deflected light, they will see a dark region where the black hole obstructs the light from the background source. This dark region is what we refer to as the shadow of the black hole. In the literature, the shadow of a black hole is defined mainly by using its photon sphere. A photon sphere is a spherical region around a black hole where photons (light particles) can orbit a black hole in a stable circular path. In [14], the authors described the shadow of a black hole as the angular diameter δ or the angular radius of the photon sphere of the same black hole.

$$\delta = 2 \arctan\left(\frac{d}{D}\right)$$

Calculating this quantity for black holes in curved spacetime requires a different approach because the original formula is designed for flat spacetime scenarios. Since our work involves curved spacetime, we will use a more appropriate formula later in the thesis to compute the black hole shadow.

1.2.1   History

- The idea of what is now known as the *shadow* of a black hole can be attributed to the work of the Irish mathematician John Lighton Synge in 1957. In his paper [15], he discussed the trajectories of light near a massive object, such as a black hole. In his work, Synge did not directly use the term *shadow* while he presenting the concept of escape cones for light[16].

- Bardeen (1973) depicted the observational insights in black holes especially shadows, in the chapter titled "Black Holes" edited by B.Dewitt and C.Dewitt [10]. He proposed the shape and size of a black hole's *shadow*, which was later made known by the observations of M87* by the Event Horizon Telescope (EHT).

- The concept that this shadow could be observed was brought forward in the year 2000 in an innovative paper by Falcke [17]. This paper highlighted the theoretical work for shadow casting by black holes because of light bending around them.

- In 2019, the Event Horizon Telescope (EHT) collaboration unveiled the first-ever image of a black hole's shadow in the center of the galaxy M87* as discussed in the above section [11].

- In 2022, the Event Horizon Telescope (EHT) captured a new image of a massive object in the center of our galaxy that which is captured in polarized light [18]. For the first time, astronomers have been capable of measuring polarization as a sign of magnetic fields, near the edge of Sagittarius A*. This image expresses the polarized view of the Milky Way black hole. The polarization is related to the magnetic field around the shadow of the black hole.

1.2.2   Shape and Size of Shadow of Black Hole

The shape and size of the black hole shadow are determined by the mass of the black hole, its spin, and the observer's viewing angle. The mass of a black hole chiefly affects the shadow of the black hole. The shadow appears larger for massive black holes, such as supermassive black holes found at the center of galaxies. The size and shape of a black hole shadow not only depend on the parameters of the black hole itself but also on the position of the observer. The spin of a black hole impacts the size and shape of its shadow. For nonrotating black holes, known as Schwarzschild black holes, the shadow is usually circular.
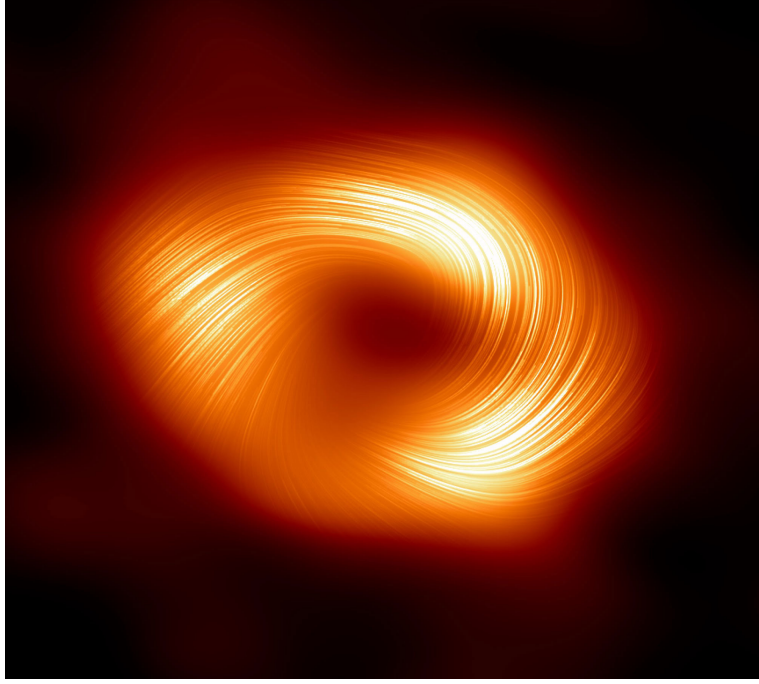
Figure 1.2. This image expresses the polarized view of the Milky Way black hole. The lines mark the alignment of polarization, which is associated with the magnetic field around the shadow of the black hole (Credit: EHT Collaboration,2022).

In contrast, for rotating black holes, or Kerr black holes, the shadow is distorted and asymmetric due to their spin.

1.2.2.1 Boundary of Black Hole Shadow

The boundary of the shadow of a black hole especially emphasizes the circular null orbits (photon spheres) by conditions given below. $\mathcal{R}(r)$ radial function or effective radial potential is specifically related to the impact parameter of photons. It represents the interaction between the angular momentum and gravitational forces of photons, influencing the formation of the shadow and the dynamics of light in the strong gravitational field of the black hole. The radial function $\mathcal{R}(r)$ is significant in observing the motion of light around black holes and defining the characteristics of shadows of black holes. For the boundary curve, there are the following conditions [19]

- $\mathcal{R}(\mathbf{r}){=}\mathbf{0}$: This condition indicates that the impact parameter at the circular null orbits is such that the particle's trajectory is a circle.

- $\frac{d}{dr}\mathcal{R}(\mathbf{r}) = \mathbf{0}$: This is associated with the gradient of the radial function. This condition at the null circular orbit depicts the trajectory that has attained an extremum. This means that the particle is neither moving inward nor outward from that specific point.

- $\frac{d^2}{dr^2}\mathcal{R}(\mathbf{r}) < \mathbf{0}$: This condition at circular null orbit assures that the circular orbit is stable against the small perturbations. If the second derivative is positive it would infer the unstable orbit where a small disturbance might lead to a particle moving away from the circular orbit.

In short, the first two conditions $\mathcal{R}(r) = 0$ and $\frac{d}{dr}\mathcal{R}(r) = 0$ primarily describe the boundary for the shadow of the black hole. The first condition gives the locations of the photon orbits and the second one suggests that orbits are critical points. The third condition just assures the stability of orbits which is important for consistency of the boundary of the shadow of the black hole.

1.2.2.2 Photon Region

The photon region is a spherical region around a black hole where photons can orbit the black hole due to its intense gravitational pull in stable or unstable paths. It plays a crucial part in casting of shadow of a black hole. The black hole shadow is the projection of the unstable photon region onto the observer's sky. When photons enter this region they may be captured or escaped by the black hole. The paths of those that are captured provide the dark silhouette seen as the black hole shadow [12].

$$r_+ < r < r_-,$$

Here the inequality indicates that the photon radius must be between two radii r_+ and r_- for the photon to remain in the photon region. In this inequality, r_+ is the radius of the prograde circular photon orbit. Prograde Orbit is referred to as orbit where light moves in the same direction as the rotation of a black hole. While r_- presents the radius of

retrograde circular photon orbit. The retrograde circular orbit is referred to as the orbit where light moves against the rotation of a black hole that we can see in Fig. (1.3) [20].
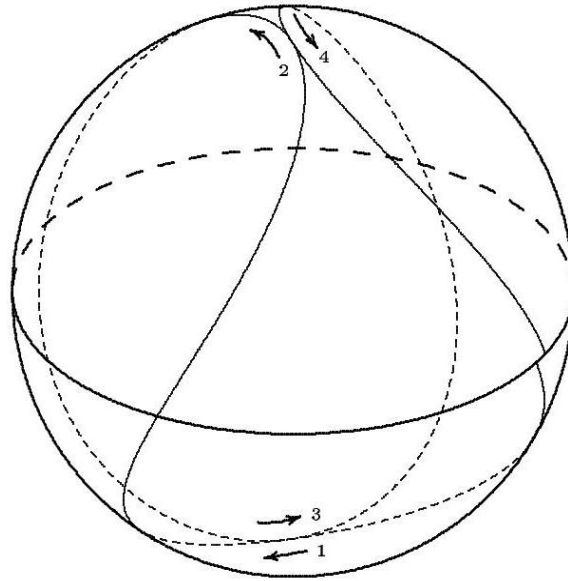
Figure 1.3. This image indicates the motion of spherical photon orbits. Here, the arrows present the direction of motion.

The inequality is important as it helps to describe the boundaries of the photon region in the context of the Kerr black hole. The presence of a photon region or photon sphere is significant in casting the shadow of the black hole, while for naked singularity it presents a completely different scenario. In the absence of a photon sphere, the naked singularities may not cast a shadow at all but in place of that, they can present an arc-shaped image where the complete region inside looks bright. That distinguishes the naked singularities from the black holes.

1.3 Shadow of Naked Singularities

As of now, Einstein's GTR is an exceptionally effective theory of gravity. A spacetime singularity would develop, according to the GTR, when masses large enough collapse under the pull of their own gravity. In 1969, Roger Penrose presented the Cosmic Censorship Conjecture (CCC), which emphasizes that horizonless strong spacetime singularities are

not feasible [21]. However, several studies on the continuous gravitational collapse of the inhomogeneous matter cloud demonstrate that spacetime singularities formed during gravitational collapse can be observed by an outside observer [22]. The conspicuousness of spacetime singularity is based on the initial conditions of the collapsing matter. In GTR, such a situation can also emerge where the continual gravitational collapse could bring about an equilibrium static spacetime with a central observable or naked singularity, such as Joshi-Malafarina-Narayan (JMN) spacetime [23]. From the above discussion, it is obvious that the naked singularity can occur as the final state of continuous gravitational collapse of an inhomogeneous matter cloud. Information about the distinguished spacetime structure near a naked singularity may be retrieved by photon trajectories. Therefore, to predict the physical signature of a naked singularity, a detailed study of null geodesics near naked singularity is very significant. A valuable approach for classifying the spacetime structure of a naked singularity to investigate the shadow of a naked singularity. The analysis of the shadow also provides an initial way of figuring out the properties of the naked singularity.

As discussed above, in 2019, the Event Horizon Telescope (EHT) group revealed the shadow image of a compact object located at the center of the M87* galaxy [24]. Besides, we also discussed above that recently the shadow image revealed by the EHT group, of a compact object located at the center of the Milky Way galaxy Sgr A*. They analyze the shadow image cast by several models and compare it to the shadow image of Sgr A*, finalizing that the JMN naked singularity is among the finest possible nonspinning black hole imitators [25]. In the literature, we can find out that, for shadow formation event horizon and photon sphere are unnecessary [26]. In [27], the authors demonstrated that the necessary and sufficient condition for shadow formation is the existence of the upper bound of effective potential of a null geodesic. Given that all compact objects in the universe naturally have intrinsic angular momentum, a rotating version of the singular static spacetime is crucial for a more realistic model. In our thesis, we will discuss the shadow geometry of Kerr naked singularity.

1.3.1 Kerr MOG Black Hole and Naked Singularities

Kerr MOG black hole solutions are obtained from the STVG field equations, which integrate a vector field alongside scalar fields to modify the gravitational interaction. Kerr MOG black hole has two horizons for $\alpha > 0$ and there is no horizon free solution with naked singularity. The Kerr MOG black hole is described by, the mass parameter $\mathcal{M}_\alpha$, the spin parameter a, and a deformation parameter α which is dimensionless [28]. The photon sphere produced by the Kerr MOG black hole is observationally distinct from the Kerr black hole, as we will see in chapter 4. The spin parameter a varies with the deformation parameter or MOG parameter α, we get some restrictions on a in MOG, given below as [29]

$$|a| < \frac{1}{\sqrt{1+\alpha}} \quad \text{Non extremal black hole,}$$
$$|a| = \frac{1}{\sqrt{1+\alpha}} \quad \text{Extremal black hole,}$$
$$|a| > \frac{1}{\sqrt{1+\alpha}} \quad \text{Naked singularity.}$$

In the above expressions, MOG parameter α must be positive definite otherwise if we invert the above inequality we get a restriction on α.

1.3.2 Scalar Tensor Vector Gravity

With remarkable advances in the accuracy of observations, Einstein's GTR has passed nearly all the tests in the solar system. However, alternative gravity theories still stand up for explaining some exotic phenomena such as dark matter(DM), and for possible violation of general relativity in future higher precision experiments. Among them, Moffat [30] presented a scalar-tensor-vector gravity (STVG) theory that has been tested in the solar system, astrophysical, and cosmological scales without dark matter [31]. The STVG

theory has three scalar fields and a vector field beside the metric tensor.

1.3.3 Plasma Around the Black Hole

Plasma is composed of charged particles, such as free electrons and positive ions. Plasma is typically generated by heating the gas or being subjected to a strong electromagnetic field, triggering the atoms to ionize. Around a black hole, the presence of plasma is a completely theoretical concept based on astrophysical observation and models. The effects of plasma on light propagation have been investigated since the 1960s. In 1966, John Ston and Muhleman explored the impact of the electronic plasma in the solar corona on the time delay of radio frequencies under the gravitational field of the sun, using the plasma and gravitational refractive indices to derive a weak field approximation [32]. Using light propagation studies on different space missions such as Viking, Mariner 6 and 7, and the Cassini mission, various analyses centered on the solar wind and the electron density profile in its outer corona were also conducted. In 1980, Ehlers and Breuer enacted a challenging derivation of a Hamiltonian for light rays consisting of magnetized plasma in a curved spacetime [33]. In literature, we can find recent work analyzing the influence of plasma on the propagation of light rays in different astrophysical situations. The EHT group recently has successfully caught a polarized light around the M87* and Sgr A*. The orientation of light waves is apparent in these polarized images, and it is influenced by the magnetic field generated by the plasma revolving around the black holes. The results from these polarized images not only assure the presence of plasma around black holes but also give observations into the mechanisms that lead to their evolution and behavior [18]. Recently, the study of shadows of different rotating spacetime under the influence of plasma, following the leading work of Volker Perlick [34].

Throughout this thesis, we will employ the convention of setting $G_N = c = 1$. This approach simplifies our analysis and facilitates the exploration of the properties and shadows associated with black holes and naked singularities. The *chapter* 1 is theoretical, It presents essential theories about black holes and the shadows they cast. The *chapter*

2 deals with the observing shadow of Kerr black hole and the naked singularity and distinguishes them from each other. This chapter provides detailed insights into how parameters such as spin and observer position influence the distinguishable features of the shadow of Kerr black hole and naked singularity. In *chapter* 3 we examine the propagation of light in plasma on Kerr spacetime and its shadow. To guarantee the separability of the Hamilton-Jacobi (HJ) equation for the light rays we find the necessary and sufficient condition of plasma density has to satisfy for which the Carter constant exists. We determine the photon region for every case in which this condition is satisfied. Then we establish an analytical expression of the boundary curve of the shadow on the observer's sky anywhere within the outer communication domain. The focus of *chapter* 4 is on the shadow of the Kerr MOG black hole and naked singularity. It also assesses the work's overall significance while offering recommendations for further research. The *chapter* 4 summarizes the results of this study and discusses the conclusion extracted from this dissertation.

Chapter 2

Shadow of a Kerr Black Hole and Kerr Naked Singularity

In this chapter, we will analyze the properties of light geodesics and the shadow around the Kerr naked singularity(KNS) and the Kerr black hole. The results indicate that the rotating Kerr naked singularity and Kerr black holes may be distinct by significant aspects such as light trajectories and the shape of shadows which provides a valuable tool differentiating a Kerr black hole from a naked singularity. Here we analyze the causal structure and some of the geometrical properties of Kerr naked Singularity spacetime. For Kerr naked singularity, the photon sphere exists only for retrograde photon orbits whereas in the case of a Kerr black hole, the photon sphere exists for both prograde and retrograde photon orbits. Consequently, an arc-shaped shadow is projected by the naked singularity that differentiates the contour-shaped shadow cast by a Kerr black hole [22].

2.1   Calculation of Shadow of Kerr Black Hole

In GTR, the Kerr metric is axially symmetric, stationary, and is a solution of Einstein's field equations. It was derived by Roy Kerr in 1963 [7]. Let's consider a Kerr black hole

14

in Boyer-Lindquist coordinates, the metric is

$$ds^2 = -\left(1 - \frac{2mr}{\rho^2}\right)dt^2 - \frac{4mra\sin^2\theta}{\rho^2}dtd\phi + \frac{\rho^2}{\Delta}dr^2 + \rho^2 d\theta^2$$
$$+ \sin^2\theta\left(r^2 + a^2 + \frac{2mra^2\sin^2\theta}{\rho^2}\right)d\phi^2, \tag{2.1}$$

and the expressions for ρ and Δ is

$$\rho^2 = r^2 + a^2\cos^2\theta,$$

$$\Delta = r^2 - 2mr + a^2,$$

where $m = \frac{G_N M}{c^2}$ is mass of gravitating body and m has dimension of unit length. The spin parameter is $a = \frac{J}{Mc}$, where J is the angular momentum of spinning black. The Kerr black hole features two separate horizons: the event horizon (outer) and the Cauchy horizon (inner), as illustrated in Fig. (2.1) [35].
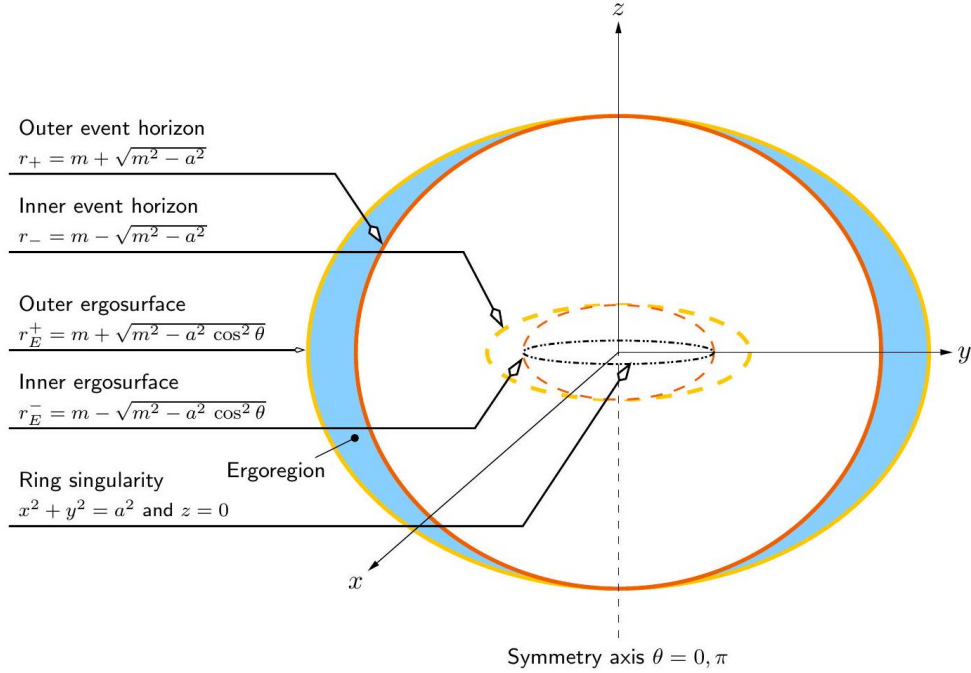
Figure 2.1. The schematic shows the positions of the horizons, ergosurfaces, and the curvature singularity in Kerr spacetime.

15

The construction of shadow in this case is more complicated. However, it can be done analytically.

2.1.1 Geodesics

There are four constants of motion which, for lightlike geodesics, are $g_{\mu\nu}\dot{x}^\mu\dot{x}^\nu = 0$ that describes the motion of light in the Kerr spacetime the Carter constant $\mathcal{C}$, the energy E, and the z component of the angular momentum L_z. Whereas E and L_z are associated with the Killing vector fields ∂_t (time translation symmetry) and ∂_ϕ (rotational symmetry around the z-axis), respectively, $\mathcal{C}$ results from the separability of the HJ equation for geodesics [36].

2.1.1.1 Killing Vectors

A Killing vector preserves the metric, as it describes the symmetries of the metric. Symmetry is defined as a coordinate transformation that does not change the form of the metric. Movement along a Killing vector field preserves the structure of the spacetime metric, meaning the metric remains unchanged in this direction. This is mathematically represented by the Killing equation, which involves covariant derivatives and is expressed as:

$$\nabla_{(a}\mathcal{X}_{b)} = 0$$

where ∇_a is the covariant derivative, and $\mathcal{X}^a$ is the Killing vector field. The equation indicates that the symmetrized covariant derivative of the Killing vector vanishes, ensuring the metric remains invariant along the vector field. The Kerr metric exhibits both axisymmetry and time translation symmetry. In these coordinates, the metric is independent of the t and ϕ components, which leads to the conservation of the associated conjugate momenta, p_t and p_ϕ [34]. These conserved quantities correspond to the constants of motion associated with the spacetime's Killing vectors.

$$\mathcal{K}^\mu = (1, 0, 0, 0) \quad R^\mu = (0, 0, 0, 1),$$

16

Accordingly, the geodesic motion in Kerr geometry is characterized by two constants of motion, which are

$$E = -\mathcal{K}^\mu p_\mu = -p_t,$$

$$L_z = R^\mu p_\mu = p_\phi. \qquad (2.2)$$

2.1.1.2 Hamilton-Jacobi Equation

In classical mechanics, you can find the equations of motion for a system by solving the (HJ) equation, which allows you to find the action function S. It provides a way to convert the problem into a form where the dynamics can easily be solved, specifically when canonical transformations are used [37]

$$H(q_i, \frac{\partial S}{\partial q_i}, t) + \frac{\partial S}{\partial t} = 0,$$

where q_i are generalized coordinates and $S = S(q_i, t)$ the action. In GTR, the motion of particles and light rays in curved spacetime can be understood with the help of the HJ equation. We can find how photons and particles move under the influence of gravitational fields by solving HJ equation. To observe the spherical photon orbits and the shadow of the Kerr black hole, we used the HJ equation [38]

$$\frac{\partial S}{\partial \lambda} = \frac{1}{2} g_{\mu\nu} \frac{\partial S}{\partial x^\mu} \frac{\partial S}{\partial x^\nu}, \qquad (2.3)$$

where S is the action as the function of affine parameter λ and coordinates x^μ.
For the separation of the HJ equation into different components we used separation ansatz,

$$S = -Et + S_r(r) + S_\theta(\theta) + L_z\phi. \qquad (2.4)$$

17

Then from the above equations, we can have equations of motion for null geodesic for each of the coordinates [36],

$$\Delta\rho^2\dot{t} = \left((r^2+a^2)^2 - \Delta a^2 \sin^2\theta\right)\mathrm{E}, \tag{2.5}$$

$$\rho^4\dot{r}^2 = \mathrm{E}^2 r^4 + (a^2\mathrm{E}^2 - \mathrm{L_z}^2 - \mathcal{C})r^2 + 2m\left((a\mathrm{E} - \mathrm{L_z})^2 + \mathcal{C}\right)r - a^2\mathcal{C}, \tag{2.6}$$

$$\rho^4\dot{\theta}^2 = \mathcal{C} - \left(\frac{\mathrm{L_z}^2}{\sin^2\theta} - \mathrm{E}^2 a^2\right)\cos^2\theta, \tag{2.7}$$

$$\Delta\rho^2\dot{\phi} = 2mraE + \left(\rho^2 - 2mr\right)\frac{\mathrm{L_z}}{\sin^2\theta}. \tag{2.8}$$

From (2.6) we can get the effective radial potential $\mathcal{R}(r)$ given as

$$\mathcal{R}(r) = r^4 + (a^2 - P^2 - Q^2)r^2 + 2mr\left((a-P)^2 + Q\right) - a^2 Q. \tag{2.9}$$

2.1.2 Spherical Photon Orbits and Shadow of Black Hole

In Kerr metric, there is no photon sphere but rather a photon region [39], also sometimes denoted as a photon shell [40]. However, a photon sphere is occupied with circular light rays, while the Kerr photon region is occupied with spherical, in general, non-planar light rays [20]. The word spherical implies that that these light rays remain on a sphere $r = const$. To find the trajectories with $r = const$. requires, the radial equation of motion that we can attain by solving the $\mathcal{R}(r) = 0$ and $\frac{d}{dr}\mathcal{R}(r) = 0$ simultaneously. Corresponding these equations we can find the following equations,

$$Q(r_{\mathrm{p}}) = \frac{4r_{\mathrm{p}}^2(r_{\mathrm{p}}^2 + a^2 - 2mr_{\mathrm{p}})}{(r_{\mathrm{p}} - m)^2}, \tag{2.10}$$

$$aP(r_{\mathrm{p}}) = \frac{-r_{\mathrm{p}}(r_{\mathrm{p}} - 3m) - r_{\mathrm{p}}a^2 - a^2 m}{r_{\mathrm{p}} - m}, \tag{2.11}$$

18

are the constant of motions, $P = \frac{L_z}{E}$ and $Q = \frac{C}{E^2}$. Here as we set the $r = r_p$ runs over the radius values of limiting spherical light rays, from its minimal value to its maximal value and back, giving us an expression for the boundary of the shadow as a curve parameterized by r_p in the form of $\chi(r_p), \psi(r_p)$.

At the position (r_0, θ_0) for an observer, we have [36]

$$\sin\chi(r_p) = \frac{Q(r_p) - a\sin^2\theta_0}{\sqrt{P(r_p)}\sin\theta_0},$$

$$\sin\psi(r_p) = \frac{\sqrt{r_0^2 + a^2 - 2mr_0}\sqrt{P(r_p)}}{r_0^2 - aQ(r_p) + a^2}. \tag{2.12}$$

For a distance observer $r_0 >> m$ the shadow formula can be simplified. Firstly, we can solve the (2.12) for $\psi(r_p)$ and then simplifying the (3.41), we get

$$x(r_p) = \frac{-Q(r_p) + a\sin^2\theta_0}{r_0\sin\theta_0}, \tag{2.13}$$

$$y(r_p) = \pm\frac{1}{r_0}\sqrt{P(r_p) - \frac{\left(Q(r_p) - a\sin^2\theta_0\right)^2}{\sin^2\theta_0}}. \tag{2.14}$$

In the observer's sky, to obtain the boundary curve of the shadow, we have to determine the corresponding constants of motion for each of the light rays issuing from the observer's position into the past.

The shadow of a Kerr black hole also a rotating one, presents distinctive aspects that differentiate it from nonrotating black holes. Kerr black hole contributes to asymmetric alterations and a horizontal displacement of the shadow, mainly for rapidly spinning black holes, as we can see in Fig. (2.1). In this figure, the shadow of Kerr black hole is seen by an equatorial observer with different spins. Curves are plotted with the help of (2.13) and (2.14). The figure shows that when we increase the value of the spin parameter, the shadow displaces horizontally its shape deformed and gives a D-shape shadow.

19
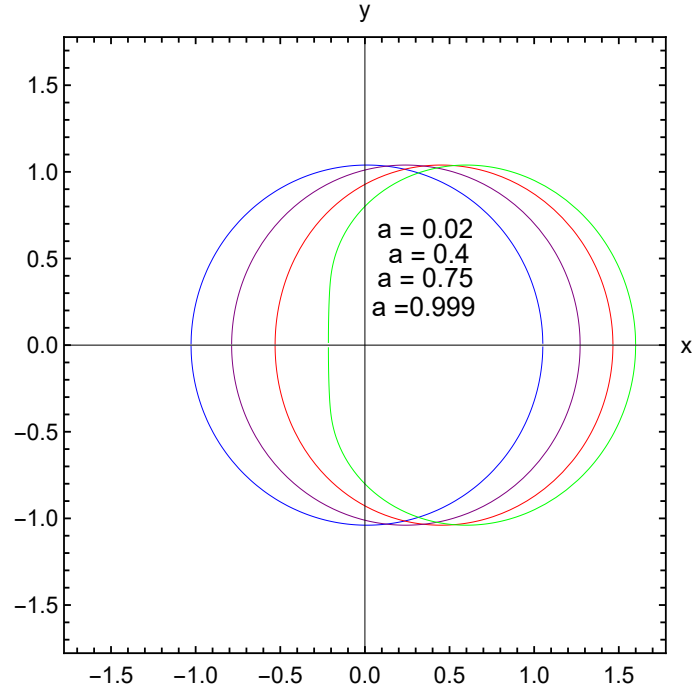
Figure 2.2. The axes in the unit of m/r_0. Kerr black hole's shadow with different spin values (from the leftmost to the rightmost),$a = 0.02m$ (blue), $a = 0.4m$ (purple), $a = 0.75m$ (red), and $a = 0.999m$ (green).
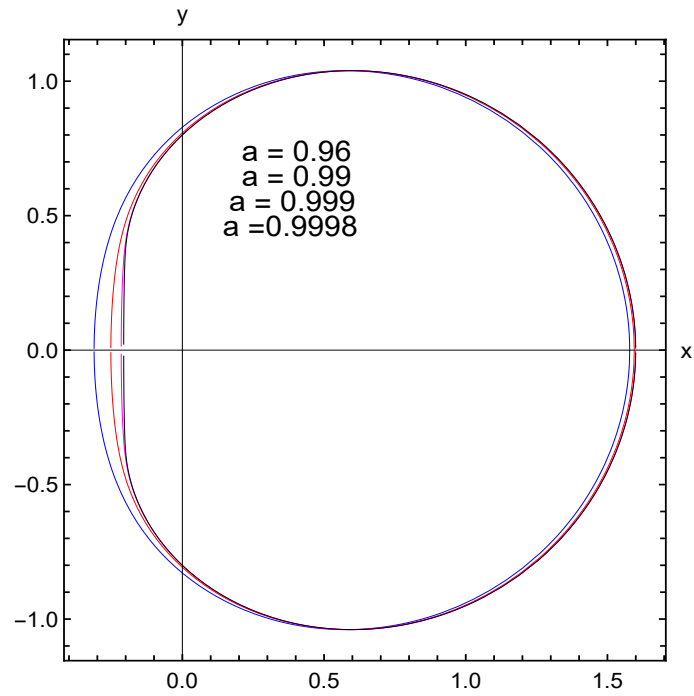
Figure 2.3. Shadow of nearly extreme Kerr black hole for different values of spin(from the leftmost to the rightmost):$a = 0.96m$, $a = 0.99m$, $a = 0.999m$ and $a = 0.9998m$.
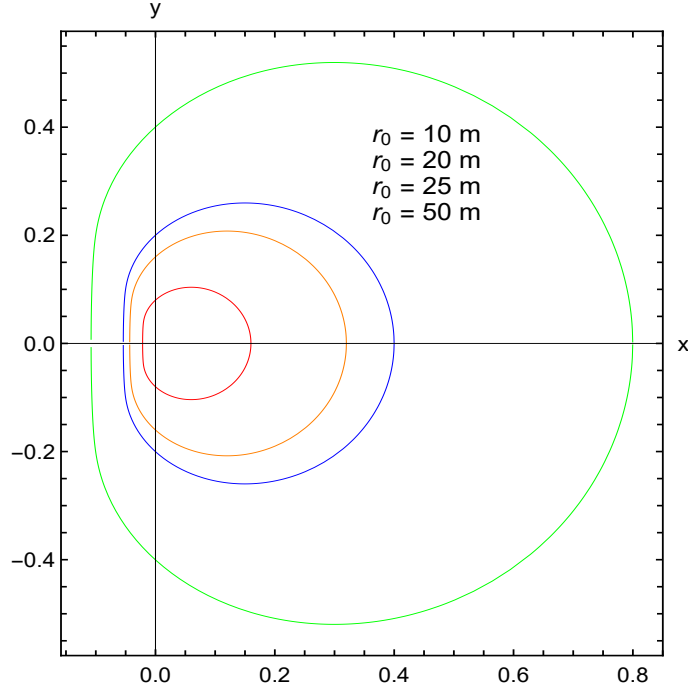
Figure 2.4. Shadow of Ker black hole as seen by different positions (from the innermost to outermost) with fixed spin $a = 0.999$: $r_0 = 10m, r_0 = 20m, r_0 = 25m, r_0 = 50m$.

In Fig. (2.2), we observe the shadow of a nearly extreme Kerr black hole. The shadow also depends on the position of the observer. In Fig. (2.3), we can see that, as the distance of observer increases, the shadow gradually diminishes in visibility and ultimately vanishes at a larger distance. The changes in shadow size and deformation, as demonstrated in the associated figures, highlight how parameters such as spin and observer position influence the distinguishable features of the shadow. These outcomes not only approve theoretical predictions but also present a foundation for further exploration into essential properties of black holes and the variant theories of gravity.

Shadow of Kerr Naked Singularities

In this section, we investigate the shadow geometry of Kerr naked singularity. We will show that the Kerr naked singularity shadow can be closed, open, or vanishing, depending on the spins and observational inclination angles. We study the critical parameters where the Kerr naked singularity shadow opens a gap, a distinctive phenomenon that does not happen with the black hole shadow [38]. The line element of Kerr metric in

Boyer-Lindquist coordinates is given by (2.1), where $a = \frac{J}{M}$ is a dimensionless spin for a Kerr compact object with angular momentum J and mass M.

For $|a| > 1$, the metric describes a Kerr naked singularity, and for $|a| < 1$ the metric describes a Kerr black hole. Without loss of generality further we consider $a > 0$. For the reason that the Kerr metric is stationary and axially symmetric, there are two Killing vectors given in section (2.1.1.1) demonstrating the time and azimuthal translation. Conserved quantities can be obtained from the symmetries of the physical laws. By projecting the Killing vectors along the covariant four-momentum vector p_μ, we find energy E and angular momentum in the ϕ direction L_z that is given in (2.2).

2.1.3 Calculation of the Shadow for Kerr Naked Singularity

To examine the spherical photon orbits and the shadow of Kerr naked singularity we use the HJ equation (2.3). The solution to (2.3) can be separated into different components depending on each coordinate, we use ansatz (2.4). The resulting equation is

$$H = \frac{1}{2} \left[\frac{-1}{\Delta} \left((r^2 + a^2) + \frac{2mra^2}{\rho^2} \sin^2 \theta \right) p_t^2 + \frac{\Delta}{\rho^2} \left(\frac{\partial S_r}{\partial r} \right)^2 + \frac{1}{\rho^2} \left(\frac{\partial S_\theta}{\partial r} \right)^2 - \frac{4mar}{\rho^2 \Delta} p_t p_\phi \right.$$
$$\left. + \frac{\Delta - a^2 \sin^2 \theta}{\Delta \rho^2 \sin^2 \theta} p_\phi^2 \right],$$

After evaluating the above equation and putting it in (2.3), we get

$$H = \frac{1}{2} \left[\frac{-1}{\Delta \rho^2} \left((r^2 + a^2)^2 - a^2 \sin^2 \theta \Delta \right) p_t^2 + \frac{\Delta}{\rho^2} S_r'(r)^2 + \frac{1}{\rho^2} S_\theta'(\theta)^2 - \frac{4mar}{\rho^2 \Delta} p_t p_\phi \right.$$
$$\left. + \frac{\Delta - a^2 \sin^2 \theta}{\Delta \rho^2 \sin^2 \theta} p_\phi^2 \right]. \tag{2.15}$$

Now, (2.4) and (2.15) yields the equations of motion for null geodesics for each of the coordinates

$$\rho^2 \Delta \dot{t} = \Xi E - 2mar L_z, \tag{2.16}$$

22

where, $\Xi = (a^2 + r^2)^2 - \Delta a^2 \sin^2 \theta$,

$$\rho^2 \Delta \dot{\phi} = 2mra\mathrm{E} + (\rho^2 - 2mr)\frac{\mathrm{L}_z}{\sin^2 \theta}, \tag{2.17}$$

$$\rho^4 \dot{\theta}^2 = \mathcal{C} - \left(\frac{\mathrm{L}_z^2}{\sin^2 \theta} - \mathrm{E}^2 a^2\right) \cos^2 \theta, \tag{2.18}$$

$$\rho^4 \dot{r}^2 = \mathrm{E}^4 r^4 + (a^2 \mathrm{E}^2 - \mathrm{L}_z{}^2 - \mathcal{C})r^2 + 2mr\left((a\mathrm{E} - \mathrm{L}_z^2 + \mathcal{C}) - a^2 \mathcal{C}\right). \tag{2.19}$$

where the over dots depict derivatives with respect to the affine parameter λ along the geodesics. The radial equation of motion (2.19) can be rewritten in terms of effective potential $\mathcal{R}(r)$ is

$$\left(\frac{\rho^2}{\mathrm{E}}\right)^2 \dot{r}^2 = -\frac{\Delta \mathcal{C}}{\mathrm{E}^2} + (r^2 + a^2)^2 - 4mar\frac{\mathrm{L}_z}{\mathrm{E}} + a^2 \frac{\mathrm{L}_z{}^2}{\mathrm{E}^2} - a^2 \Delta - \left(\frac{\mathrm{L}_z}{\mathrm{E}}\right)^2 \Delta, \tag{2.20}$$

$$\left(\frac{\rho^2}{\mathrm{E}}\right)^2 \dot{r}^2 = r^4 + a^2(a^2 - \varphi^2 - \mathcal{C}) + 2mr\left((a - \varphi)^2 + \mathcal{C}\right) - a^2 \zeta. \tag{2.21}$$

Thus, we describe the impact parameters $\varphi = \frac{\mathrm{L}_z}{\mathrm{E}}$ and $\zeta = \frac{\mathcal{C}}{\mathrm{E}^2}$ where $\mathcal{C}$ is Carter's constant, a third conserved quantity derived by the separability of HJ equation. $\mathcal{C}$ is related to geodesics in the latitudinal direction. Now the effective potential by the radial equation of motion is

$$\mathcal{R}(r) = r^4 + a^2(a^2 - \varphi^2 - \zeta) + 2mr\left((a - \varphi)^2 + \zeta\right) - a^2 \zeta. \tag{2.22}$$

2.1.4 Spherical Photon Orbits and Shadow

We get the two sets of solutions after solving the $\mathcal{R}(r) = \frac{d}{dr}(\mathcal{R}) = 0$ for spherical photon orbits with constant radius $r = r_{\mathrm{p}}$. However, only one solution is physical and thus

23

related to our calculations [20].

$$\varphi = \frac{a^2 m + a^2 r_{\mathrm{p}} - 3r_{\mathrm{p}}^2 + r_{\mathrm{p}}^3}{a(m - r_{\mathrm{p}})}, \tag{2.23}$$

$$\zeta = -\frac{r_{\mathrm{p}}^3(-4a^2 m + 9m^2 r_{\mathrm{p}} - 6mr_{\mathrm{p}}^2 + r_{\mathrm{p}}^3)}{a^2(m - r_{\mathrm{p}})^2}. \tag{2.24}$$

The impact parameters φ and ζ are significant in finding the shape of the shadow. We can find stable and unstable photon orbits around the Kerr naked singularity. In the context of Kerr naked singularity, a single photon sphere for retrograde motion presents a specific critical impact parameter that describes the boundary between captured light and light that is escaped by the singularity that we can see in Fig. (2.4).

This figure presents the behavior of φ and ζ as a function of r, where we take $a = 1.38$ and $M = 1$. Orbits with a positive φ value depict the prograde equatorial motion of photons, and those with a negative φ value describe the retrograde equatorial orbit. For Kerr naked singularity, ζ_{KNS} disappears at $r_{\mathrm{ph}} = 4.32$ as presented in Fig. (2.4). Corresponding to this radius the circular orbit is retrograde, since φ_{KNS} is negative at $r_{\mathrm{ph}} = 4.32$, and we identify that for the prograde equatorial motion of photons, no photon sphere exists. Unstable photon orbits surrounding Kerr naked singularity exist in the range $r_{\mathrm{ms}} < r_{\mathrm{p}} < r_{\mathrm{ph}}$ where r_{ms} is a marginally stable radius and r_{ph} is the equatorial retrograde circular radius that we can get numerically by putting $\zeta = 0$, also can be seen in Fig. (2.4).

Hence, the corresponding critical impact parameter is $\varphi_{\mathrm{KNS}} = 7.68$, there is only one photon sphere $r_{\mathrm{ph}} = 4.32$ for the retrograde motion of null geodesics in Kerr naked singularity spacetime. The marginally stable radius r_{ms} can be calculated as [41].

$$\frac{d^2}{dr^2}\mathcal{R}(r) = 0. \tag{2.25}$$

Which yield,
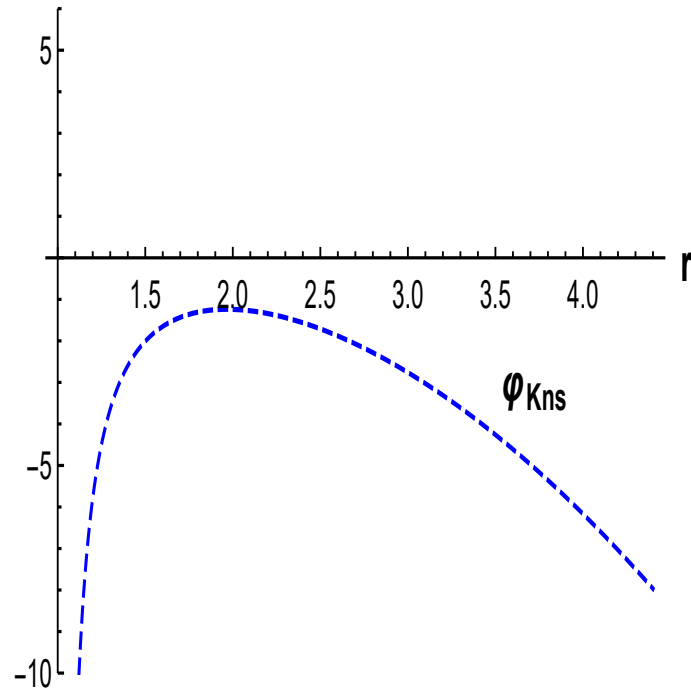
Figure 2.5. This figure demonstrates the behavior of φ for the Kerr naked singularity as a function of radial coordinate r. Here, we take $a = 1.38$ and $m = 1$.
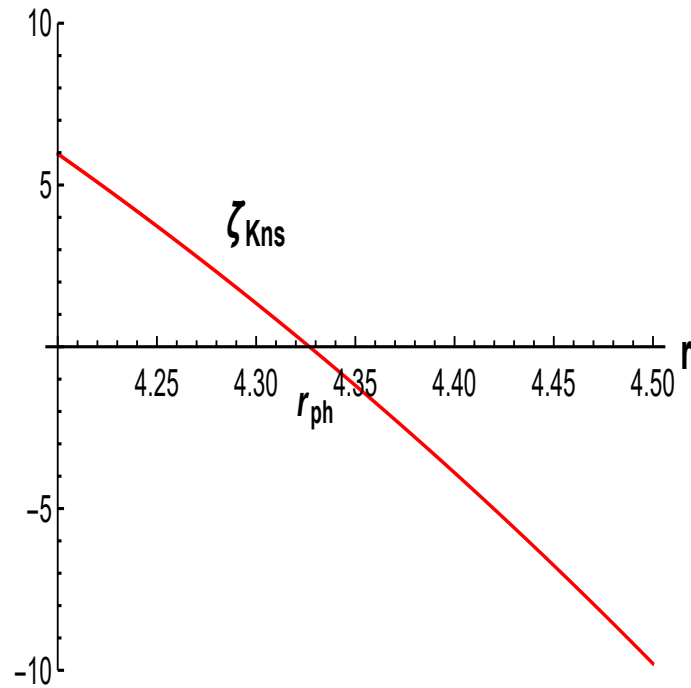
Figure 2.6. This figure depicts the behavior of ζ for the Kerr naked singularity as a function of radial coordinate r. Here, we take $a = 1.38$ and $m = 1$.

$$r_{\mathrm{ms}} = m + (a^2 m - m^3)^{\frac{1}{3}}. \tag{2.26}$$

While stable photon orbits with $r < r_{ms}$ are normally concealed inside the event horizon for the Kerr black hole, they have physical importance for Kerr naked singularity because of the absence of an event horizon. However, bounded photon orbits cannot be observed by distant observers, so they are unrelated to our study of the observational aspects of Kerr naked singularity [38].

We can obtain the apparent shape of the shadow seen by the asymptotic observer if we consider the celestial coordinates σ and τ, which are the coordinates of the asymptotic observer's sky. The general expression to find celestial coordinates σ and τ are [38],

$$\sigma = \lim_{r_0 \to \infty} \left(-r_0^2 \sin \mathrm{i} \frac{d\Psi}{dr}\big|_{r_0,\mathrm{i}} \right) = -\varphi \csc \mathrm{i}, \tag{2.27}$$

$$\tau = \lim_{r_0 \to \infty} \left(r_0^2 \frac{d\Phi}{dr}\big|_{r_0,\mathrm{i}} \right) = \pm \left(\zeta + a^2 \cos^2 \mathrm{i} - \varphi^2 \cot^2 \mathrm{i} \right)^{\frac{1}{2}}. \tag{2.28}$$

These parameters are relevant to the image plane at infinity with orthogonal coordinates σ and τ which perceive the Kerr naked singularity at a polar inclination angle i. According to (2.27) and (2.28), Figs. (2.5) to (2.9) represent the analytical Kerr naked singularity shadow by projecting the unstable photon orbits to an image plane at infinity with orthogonal coordinates σ and τ for different values of spin a and inclination angle i.

In Fig. (2.5) we can see that for smaller inclination angles such as i = 15° (closer to viewing), the shadow of Kerr naked singularity opens its gap at a greater spin and vanishes at $a = 1.404m$. However, in Figs. (2.6) and (2.7) the shadow of Kerr naked singularity at greater inclination angles do not vanish at a smaller spin such as in Fig. (2.5). Further, the Figs. (2.8) and (2.9) depict that the closed shadow is only possible

26
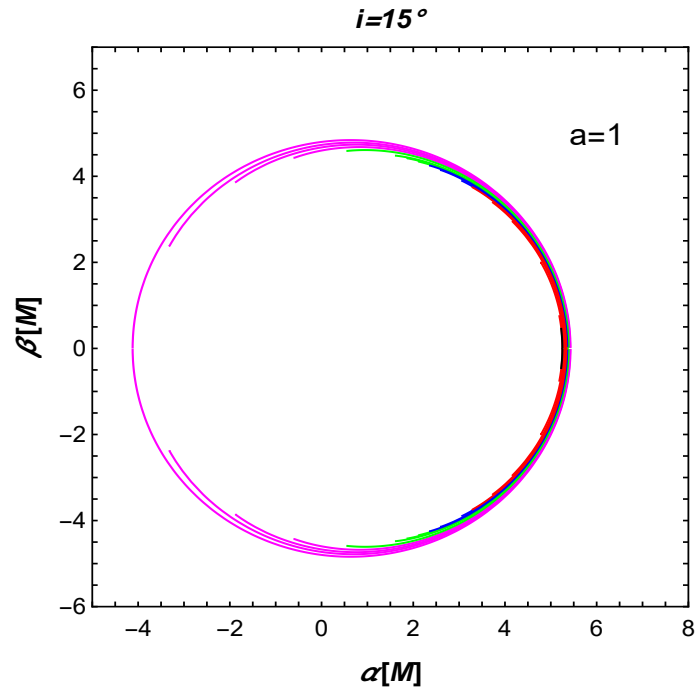
Figure 2.7. Shadows of Kerr naked singularity with observational inclinations angles
"i" and spins "a". This plot is associated with i $=$ 15°. In the plot, different colors
correspond to different spins, ranging from magenta being $a = 1.02$ to being black $a =$
1.402 .
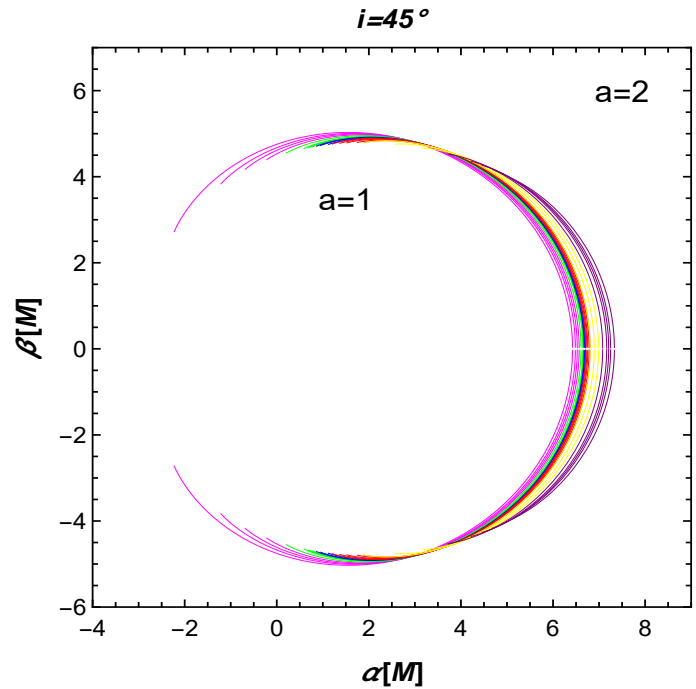
Figure 2.8. This plot is associated with i $=$ 45° In the plot, different colors correspond
to different spins, ranging from magenta $a = 1.02$ to purple $a = 2$.
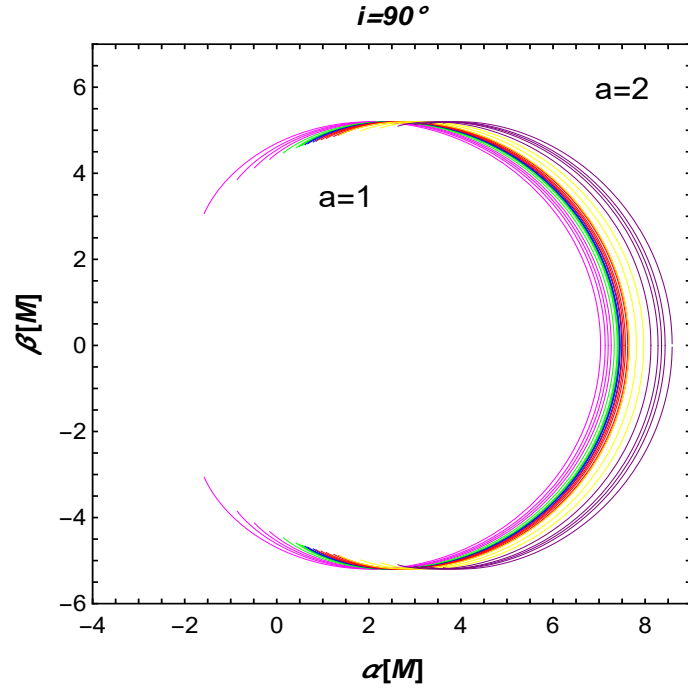
Figure 2.9. This plot is associated with i $= 90°$. In the plot, different colors correspond to different spins, ranging from magenta $a = 1.02$ to purple $a = 2$.
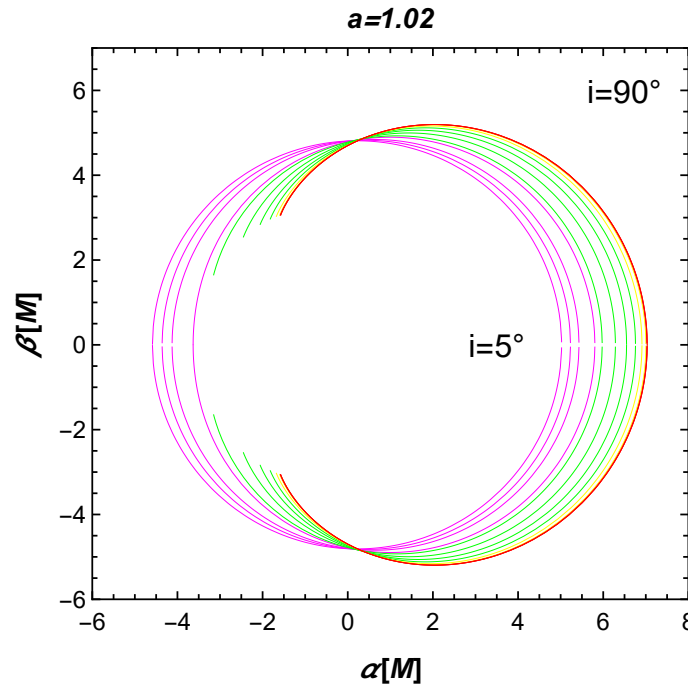
Figure 2.10. This plot corresponds to $a = 1.02$ and different colors correspond to different inclination angles, ranging from magenta i $= 5°$ (face-on).
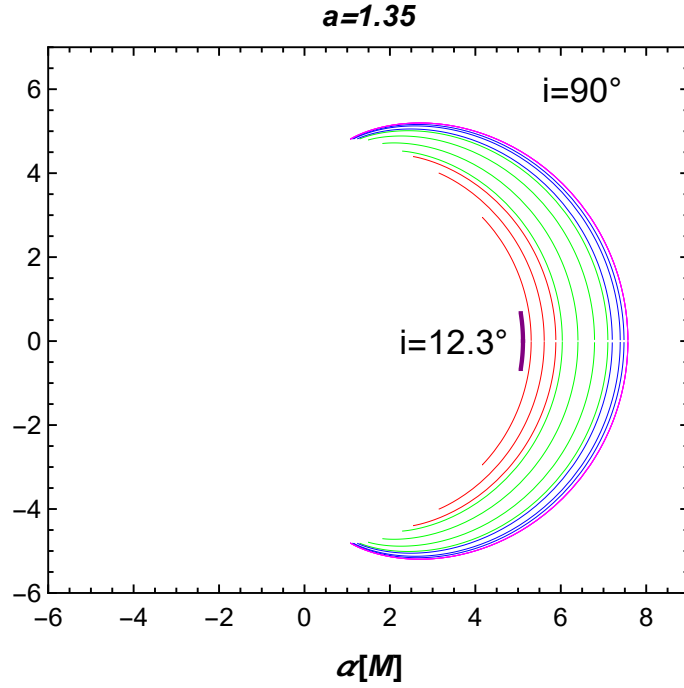
Figure 2.11. This plot corresponds to $a = 1.35$ and different colors correspond to different inclination angles, ranging from magenta being i $= 90°$ (edge-on).

with the smaller inclination angle and spin range from $1 < a \lesssim 1.18$. When $a \approx 1.18$ the shadow is open with the gap for every inclination angle but with greater spin than $a \approx 1.18$ the shadow disappears at smaller inclination angles [38]. In this chapter, we discussed the shadow of the Kerr black hole and naked singularity. We can see that because of the specific geometry of the photon sphere around Kerr naked singularity, it casts the arc-shaped shadow we can see in Fig. (2.9) while the shadow of Kerr Black can be seen in Fig. (2.2). The shadow of Kerr naked singularity is nearly half of that of the Kerr black hole. With the increasing spin, the deformation in the shadow shape of the Kerr black hole increases whereas the shadow size in Kerr naked singularity decreases.

Chapter 3

Shadow of Kerr Black Hole in the Presence of Plasma

In this chapter, we will focus on the shadow of a Kerr black hole under the influence of plasma. We study light propagation through a plasma medium. There are used particular plasma distributions, which make the whole analysis analytically manageable. We will discuss an analytical formula following [34] outside the horizon of the Kerr black hole in the presence of plasma for the boundary curve of shadow at any arbitrary point. When we consider homogeneous and inhomogeneous plasma distributions, the distortions in the shadow contour differ, and we compare them with the distinguished shadow structures of the Kerr black hole. Our settlements are as follows. We use the summation convention for Greek indices that take 0, 1, 2, and 3. Our choice of signature is $(-, +, +, +)$. We raise and lower Greek indices with the spacetime metric. G_N is the gravitational constant and c is speed of light in a vacuum. We use units such that $\hbar = 1$, as momentum vectors have the same unit as wave vectors and energies have the same unit as frequencies [34].

3.1 Hamilton Approach for the Light Rays on Kerr Spacetime in Plasma

The Hamiltonian formulation that describes the light propagation in a non-magnetized pressureless plasma [42] is,

$$H(x,p) = \frac{1}{2}\left(g^{\mu\nu}(x)p_\mu p_\nu + \omega_{\rm p}(x)^2\right).$$

(3.1)

where

$x^\mu = \left(x^0, x^1, x^2, x^3\right)$ spacetime coordinates,

$p_\mu = (p_0, p_1, p_2, p_3)$ canonical momentum coordinates,

$g^{\mu\nu} =$ contravariant components of the spacetime,

$\omega_{\rm p} =$ plasma electron frequency.

Mathematically, plasma frequency is

$$\omega_{\rm p}(x) = \frac{4\pi e^2}{m} N_{\rm e}(x),$$

(3.2)

where m is the mass of the electron, $N_{\rm e}$ is electron number density and e is the electric charge. In the case of a vacuum, the plasma frequency is defined as $\omega_{\rm p}(x) = 0$. A plasma is a dispersive medium with an index of refraction [34]

$$n(x,\omega)^2 = 1 - \frac{\omega_{\rm p}(x)^2}{\omega(x)^2},$$

(3.3)

which depends on $\omega(x)$ (photon frequency) concerning plasma frequency. In this medium

light propagation is possible only if [43]

$$\omega_{\mathrm{p}}(x) \leq \omega(x), \tag{3.4}$$

which assures a nonnegative and real index of refraction. The Hamiltonian represents the total energy of the system. For light rays the equation of motions that is derived from Hamilton's equations [34],

$$\frac{dx^\mu}{ds} = \frac{\partial H}{\partial p_\mu}, \quad \frac{dp_\mu}{ds} = -\frac{\partial H}{\partial x^\mu}, \quad H(x,p) = 0,$$

where s is the arc length. $H(x,p) = 0$ shows that the Hamiltonian is conserved along the trajectory of light. To illustrate the behavior of light in the gravitational field, we set $H(x,p) = 0$ and compute the constant of motions. These constants comprise the angular momentum, which is mainly significant in axisymmetric spacetimes like Kerr metric, and the energy that is related to the motion of light.

3.2   Hamiltonian with Kerr Metric Coefficients

From (3.1), we obtain the following expression for Hamiltonian, given below

$$H(x,p) = \frac{1}{2} \left[\frac{-1}{\Delta c^2 \rho^2} \left((r^2 + a^2)\rho^2 + 2mra^2 \sin^2\theta \right) p_{\mathrm{t}}^2 + \frac{\Delta}{\rho^2} p_{\mathrm{r}}^2 + \frac{1}{\rho^2} p_\theta^2 - \frac{4mar}{c\rho^2 \Delta} p_{\mathrm{t}} p_\phi \right.$$
$$\left. + \frac{\Delta - a^2 \sin^2\theta}{\Delta \rho^2 \sin^2\theta} p_\phi^2 + \omega_{\mathrm{p}}(r,\theta)^2 \right], \tag{3.5}$$

Simplifying this equation leads us to the following result

$$H = \frac{1}{2\rho^2} \left[\frac{-1}{\Delta} \left((r^2 + a^2)\frac{p_{\mathrm{t}}}{c} + ap_\phi \right)^2 + \left(\frac{p_\phi}{\sin\theta} + a\sin\theta \frac{p_{\mathrm{t}}}{c} \right)^2 + \Delta p_{\mathrm{r}}^2 + p_\theta^2 + \rho^2 \omega_{\mathrm{p}}(r,\theta)^2 \right]. \tag{3.6}$$

This is the Hamiltonian with Kerr metric coefficients. If we suppose that ω_p only depends on r and θ, than $\frac{\partial H}{\partial t} = 0$ and $\frac{\partial H}{\partial \phi} = 0$ which implies that p_t and p_ϕ are constant of motions. p_ϕ is angular momentum and $p_\mathrm{t} = c\omega_0$ where ω_0 is the frequency of photons as measured by a stationary observer at infinity [34].

3.3 Separability of Hamilton-Jacobi Equation for Light Rays

We have three constants of motion for light rays if ω_p only depends on r and θ, then they are

$$H = 0, \quad p_\mathrm{t} = c\omega_0 \quad and \quad p_\phi.$$

Next, we will investigate the particular form of the function $\omega_\mathrm{p}(r, \theta)$ for which the HJ equation can be separated. From this, we can get the fourth constant of motion for which the equation of motion for light rays becomes completely integrable. By (3.6), the HJ equation

$$0 = H\left(x, \frac{\partial S}{\partial x}\right), \tag{3.7}$$
$$p_\phi = \frac{\partial S}{\partial \phi}, \quad p_\theta = \frac{\partial S}{\partial \theta}.$$

By inserting the previously mentioned expressions into (3.6), we get

$$0 = \frac{1}{2\rho^2}\left[-\frac{1}{\Delta}\left(a\frac{\partial S}{\partial \phi} + (r^2 + a^2)\frac{1}{c}\frac{\partial S}{\partial t}\right)^2 + \left(\frac{1}{\sin\theta}\frac{\partial S}{\partial \phi} + \frac{a}{c}\sin\theta\frac{\partial S}{\partial t}\right)^2 \right.$$
$$\left. + \left(\frac{\partial S}{\partial \theta}\right)^2 + \Delta\left(\frac{\partial S}{\partial r}\right)^2 + \rho^2\omega_\mathrm{p}^2\right],$$

$$0 = -\frac{1}{\Delta} \left(a \frac{\partial S}{\partial \phi} + \left(r^2 + a^2 \right) \frac{1}{c} \frac{\partial S}{\partial t} \right)^2 + \left(\frac{1}{\sin \theta} \frac{\partial S}{\partial \phi} + \frac{a}{c} \sin \theta \frac{\partial S}{\partial t} \right)^2$$
$$+ \left(\frac{\partial S}{\partial \theta} \right)^2 + \Delta \left(\frac{\partial S}{\partial r} \right)^2 + \rho^2 \omega_{\mathrm{p}}^2. \tag{3.8}$$

Now, by using separation ansatz

$$S(t, r, \theta, \phi) = c\omega_0 t + S_r(r) + S_\theta(\theta) + p_\phi \phi. \tag{3.9}$$

By substituting the $S'_\theta(\theta) = \frac{\partial S}{\partial \theta}$ and $S'_r(r) = \frac{\partial S}{\partial r}$ into (3.6), we obtain the following

$$0 = -\frac{1}{\Delta} \left(ap_\phi + \left(r^2 + a^2 \right) \omega_0 \right)^2 + \left(\frac{p_\phi}{\sin \theta} + a \sin \theta \omega_0 \right)^2 + \Delta S'_r(r)^2 + S'_\theta(\theta)^2$$
$$+ \omega_{\mathrm{p}}^2 \left(r^2 + a^2 \cos^2 \theta \right). \tag{3.10}$$

The separability of the HJ equation requires that (3.8) must be arranged such that the right-hand side is independent of θ while the left-hand side is independent of r. From (3.8) it can be seen that this is possible if and only if plasma frequency is of the form [34]

$$\omega_{\mathrm{p}}(r, \theta)^2 = \frac{f_{\mathrm{r}}(r) + f_\theta(\theta)}{r^2 + a^2 \cos^2 \theta}, \tag{3.11}$$

with some function $f_{\mathrm{r}}(r)$ and $f_\theta(\theta)$. By putting (3.9) in (3.8), we get

$$S'_\theta(\theta)^2 + \left(\frac{p_\phi}{\sin \theta} + a \sin \vartheta \omega_0 \right)^2 + f_\theta(\theta) =$$
$$-\Delta S'_r(r)^2 + \frac{1}{\Delta} \left(ap_\phi + \left(r^2 + a^2 \right) \omega_0 \right)^2 - f_{\mathrm{r}}(r) =: \mathcal{C}. \tag{3.12}$$

As the first expression is independent of r and the second one is independent of θ, the quantity $\mathcal{C}$ is a constant as it does not depend on r and θ. $\mathcal{C}$ is the generalized Carter constant. Through $S'_r(r) = p_r$ and $S'_\theta(\theta) = p_\theta$, we find that

$$p_\theta^2 = \mathcal{C} - \left(\frac{p_\phi}{\sin \theta} + a \sin \theta \omega_0 \right)^2 - f_\theta(\theta), \tag{3.13}$$

$$\Delta p_r^2 = -\mathcal{C} + \frac{1}{\Delta} \left(\left(r^2 + a^2 \right) \omega_0 + a p_\phi \right)^2 - f_{\rm r}(r). \tag{3.14}$$

3.3.1 Equations of Motion for the Light Rays

Inserting the expressions of p_θ and $p_{\rm r}$ into Hamilton's equations

$$\dot{x}^\mu = \frac{\partial H}{\partial p_\mu}, \tag{3.15}$$

where $x^\mu = \theta$ and $x^\mu = r$, respectively. By using (3.13) for $x^\mu = \theta$, we get

$$\dot{\theta} = \frac{\partial H}{\partial p_\theta} = \frac{1}{\rho^2} p_\theta,$$

$$\rho^4 \dot{\theta}^2 = \mathcal{C} - \left(\frac{p_\phi}{\sin\theta} + a \sin\theta \omega_0 \right)^2 - f_\theta(\theta). \tag{3.16}$$

Similarly, we will refer to equation (3.14) for $\dot{r}$ which leads to

$$\rho^4 \dot{r}^2 = \Delta^2 p_r^2,$$

$$\rho^4 \dot{r}^2 = \Delta \left(-\mathcal{C} + \frac{1}{\Delta} \left(\left(r^2 + a^2 \right) \omega_0 + a p_\phi \right)^2 - f_{\rm r}(r) \right) =: \mathcal{R}(r). \tag{3.17}$$

The other two components are $x^\mu = t$ and $x^\mu = \phi$. Now, we are proceeding for $\dot{\phi}$.

$$\rho^2 \dot{\phi} = \frac{-a}{\Delta} \left(a p_\phi + (r^2 + a^2)\omega_0 \right) + \frac{p_\phi + a \sin^2\theta\omega_0}{\sin^2\theta}, \tag{3.18}$$

$$\rho^2 \dot{\phi} = \frac{-2mra\omega_0\theta \sin^2\theta + \left(\rho^2 - 2mr \right) p_\phi}{\Delta \sin^2\theta}. \tag{3.19}$$

From the same expression, solving for $\dot{t}$, we find

$$\rho^2 \dot{t} = -\frac{1}{\Delta c} \left[\left(a p_\phi + \left(a^2 + r^2 \right) \frac{p_{\rm t}}{c} \right) + (a^2 + r^2) \right] + 2 \left[\left(\frac{p_\phi}{\sin\theta} + \frac{a \sin\theta p_{\rm t}}{c} \right) \frac{a \sin\theta}{c} \right],$$

$$\rho^2 \dot{t} = \left[\frac{-\left(ap_\phi + \left(a^2 + r^2\right)\omega_0\right)\left(a^2 + r^2\right) + a\left(p_\phi + a\sin^2\theta\omega_0\right)\Delta}{c\Delta} \right],$$

Ultimately, we find the equation to be

$$\rho^2 \dot{t} = \frac{-\left(\left(r^2 + a^2\right)\rho^2 + 2mra^2\sin^2\theta\right)\omega_0 - 2mrap_\phi}{c\Delta}. \tag{3.20}$$

Then, (3.16),(3.17),(3.18), and (3.20) give us the equation of motions for the rays in the first-order form. In short, we found that the (3.11) condition is necessary and sufficient for a generalized Carter constant to guarantee the complete integrability of the equations of motion. Next, we will calculate the photon region and the shadow, and for these calculations (3.11) must be satisfied for the existence of the Carter Constant. This mathematical method will not work for the other plasma densities.

3.3.2   Index of Refraction

The separability condition (3.11) in terms of the index of refraction (3.3) is [42]

$$n(x, \omega(x))^2 = 1 - \frac{f_{\rm r}(r) + f_\theta(\theta)}{\omega(x)^2 \rho^2}. \tag{3.21}$$

In the case of homogeneous plasma, with $\omega_{\rm p} = \omega_{\rm c}=$ (const.), the relation in (3.11) is satisfying the following [34]

$$f_{\rm r}(r) = \omega_{\rm c}^2 r^2, \, f_\theta(\theta) = \omega_{\rm c}^2 a^2 \cos^2\theta. \tag{3.22}$$

3.4   Photon Regions in a Plasma on the Kerr Spacetime

To write the θ and r components of the ray equation in separable forms see (3.16) and (3.17), we consider a plasma distribution in the form of (3.11).

The region in spacetime filled with spherical light rays is the photon region, for example

with the solutions to the ray equation that remains on a sphere $r = const.$ (in Boyer Lindquist coordinates). Light rays approaching unstable spherical light sources in a spiral motion may serve as limit curves. In the next section, we will see its importance for the construction of shadows. Spherical light rays satisfy the conditions $\dot{r} = 0$ and $\ddot{r} = 0$, as described in the notation of (3.17)

$$0 = \mathcal{R}(r) = -\left((\mathcal{C} + f_r(r))\Delta + \left(r^2 + a^2 \right)\omega_0 + ap_\phi \right)^2, \tag{3.23}$$

$$0 = \mathcal{R}(r) = -\left((\mathcal{C} + f_r(r))(r^2 + a^2 - 2mr) + \left(r^2 + a^2 \right)\frac{p_t}{c} + ap_\phi \right)^2,$$

Taking the derivative of above expression w.r.t. r:

$$0 = \mathcal{R}'(r) = -(\mathcal{C} + f_r(r))2(r - m) - f_r'(r)\Delta + \frac{4rp_t}{c}\left((r^2 + a^2)\omega_0 + ap_\phi \right). \tag{3.24}$$

Equations (3.23) and (3.24) solved for constants of motion $\mathcal{C}$ and ap_ϕ. Now, through solving (3.23)

$$(\mathcal{C} + f_r(r))\Delta = \left(\left(r^2 + a^2 \right)\omega_0 + ap_\phi \right)^2,$$

Expanding this equation leads to

$$\left(\mathcal{C} + f_r(r) \right)\Delta = \left(\left(r^2 + a^2 \right)\omega_0 \right)^2 + a^2 p_\phi^2 + 2\omega_0 \left(r^2 + a^2 \right)ap_\phi,$$

By using above expression in (3.24), we get

$$\left(\mathcal{C} + f_r(r) \right)2(r - m) = 4r\omega_0 \left(\left(r^2 + a^2 \right)\omega_0 + ap_\phi \right) - f_r'(r)\Delta,$$

$$\mathcal{C} + fr(r) = \frac{2r\omega_0}{(r - m)}\left(\left(r^2 + a^2 \right)\omega_0 + ap_\phi \right) - \frac{f'(r)\Delta}{2(r - m)}.$$

37

Multiplying by Δ, then substitute the value of $(k + f_r(r))\Delta$ derived from (3.23) leads to

$$\left(\left(r^2 + a^2\right)\omega_0\right)^2 + a^2 p_\phi^2 + 2\left(r^2 + a^2\right)\omega_0 a p_\phi = \frac{2r\omega_0\Delta}{r - m}\left(\left(r^2 + a^2\right)\omega_0 + a p_\phi\right) - \frac{f'(r)\Delta^2}{2(r - m)},$$

or

$$a^2 p_\phi^2 + \left(2\left(r^2 + a^2\right)\omega_0 - \frac{2r\omega_0\Delta}{r - m}\right)a p_\phi + \left(\left(r^2 + a^2\right)\omega_0\right)^2 - \frac{2r\omega_0\Delta}{r - m}\left(\left(r^2 + a^2\right)\omega_0\right)$$
$$+ \frac{f'(r)\Delta^2}{2(r - m)} = 0.$$

We will now proceed to compute $a p_\phi$

$$a p_\phi = \frac{1}{2}\left[-\left(2\left(r^2 + a^2\right)\omega_0 - \frac{2r\omega_0\Delta}{r - m}\right) \pm \left(\left(2\left(r^2 + a^2\right)\omega_0 - \frac{2r\omega_0\Delta}{r - m}\right)^2\right.\right.$$
$$\left.\left. -4\left(\left(\left(r^2 + a^2\right)\omega_0\right)^2 - \frac{2r\omega_0\Delta}{r - m}\left(\left(r^2 + a^2\right)\omega_0\right) + \frac{f'(r)\Delta^2}{2(r - m)}\right)\right)^{1/2}\right],$$

The resulting expression for $a p_\phi$ is given by

$$a p_\phi = \frac{\omega_0}{r - m}\left[\left(a^2 - r^2\right)m \pm \Delta r\sqrt{1 - \frac{f'(r)(r - m)}{2r^2\omega_0^2}}\right]. \tag{3.25}$$

Next, we will evaluate the (3.23) for value of $\mathcal{C}$

$$(\mathcal{C} + f_r(r))\Delta = \left(\left(r^2 + a^2\right)\omega_0 + a p_\phi\right)^2,$$

Substituting the above equation into (3.25),to get

$$(\mathcal{C} + f_r(r))\Delta = \left[\left(r^2 + a^2\right)\omega_0 + \frac{\omega_0}{r - m}\left(\left(a^2 - r^2\right)m \pm \Delta r\sqrt{1 - \frac{f'(r)(r - m)}{2r^2\omega_0^2}}\right)\right]^2,$$

38

The resulting expression takes the form

$$\mathcal{C} = \frac{\omega_0^2 r^2 \Delta}{(r-m)^2} \left[1 \pm \sqrt{1 - \frac{f'(r)(r-m)}{2r^2\omega_0^2}} \right]^2 - f_{\rm r}(r). \tag{3.26}$$

As the left-hand side of (3.20) is the square of a real quantity, the right-hand side must be non-negative. From (3.16), it follows that

$$0 \le \mathcal{C} - \left(\frac{p_\phi}{\sin\theta} + a\sin\theta\omega_0 \right)^2 - f_\theta(\theta),$$

and hence we obtain the inequality

$$0 \le \mathcal{C}\sin\theta - f_\theta(\theta)\sin\theta - \left(p_\phi + a\omega_0\sin^2\theta \right)^2,$$

$$\left(\mathcal{C} - f_\theta(\theta) \right)\sin\theta \ge \left(p_\phi + a\omega_0\sin^2\theta \right)^2. \tag{3.27}$$

On substituting the (3.25) and (3.26) into above equation, gives the photon region

$$\left(\frac{r^2\Delta}{(r-m)^2} \left(1 \pm \sqrt{1 - f'_{\rm r}(r)\frac{(r-m)}{2r^2\omega_0^2}} \right)^2 - \frac{f_{\rm r}(r) + f_\theta(\theta)}{\omega_0^2} \right) a^2\sin^2\theta \ge$$

$$\left(\frac{1}{(r-m)} \left(m\left(a^2 - r^2\right) \pm r\Delta\sqrt{1 - f'_{\rm r}(r)\frac{(r-m)}{2r^2\omega_0^2}} \right) + a^2\sin^2\theta \right)^2.$$

So, the region where this inequality is satisfied through each point with coordinates (r, θ), either with the minus or plus sign, there is a spherical light ray. Generally, the photon region consists of stable and unstable spherical light rays. As discussed above the unstable spherical light rays must have

$$0 < \mathcal{R}''(r) = -2\mathcal{C} - 2f_{\rm r}(r) + 4\omega_0 \left(\left(r^2 + a^2\right)\omega_0 + ap_\phi \right)$$

$$+ 8r^2\omega_0^2 - f'_{\rm r}(r)4(r-m) - f''_{\rm r}(r)\Delta. \tag{3.28}$$

where $\mathcal{C}$ and ap_ϕ should be expressed in terms of the frequency ω_0 and the radius r with the help of (3.25) and (3.26).

3.5 Calculation of Shadow of Kerr Black Hole in Plasma

Now we calculate the boundary curve of the shadow on the observer's sky then we fix an observer at Boyer Lindquist coordinates (r_0, θ_0) with $r_0 > m + \sqrt{m^2 - a^2}$. The observation events t and ϕ coordinates are irrelevant because of the symmetries of the metric. We select an orthonormal tetrad [44],

$$
\begin{aligned}
\hat{e}_0 &= \left. \frac{\left(r^2 + a^2\right)\partial_t + ac\partial_\phi}{c\rho\sqrt{\Delta}} \right|_{(r_0,\theta_0)}, \\
\hat{e}_1 &= \left. \frac{1}{\rho}\partial_\theta \right|_{(r_0,\theta_0)}, \\
\hat{e}_2 &= \left. \frac{-\partial_\phi - a\sin^2\theta\partial_t}{\rho\sin\vartheta} \right|_{(r_0,\theta_0)}, \\
\hat{e}_3 &= \left. -\frac{\sqrt{\Delta}}{\rho}\partial_r \right|_{(r_0,\theta_0)}.
\end{aligned}
\tag{3.29}
$$

This tetrad is orthonormal and well-defined for any observer position in the domain of outer communication. The timelike vector $\hat{e}_0$ is to be interpreted as the four-velocity of our observer.It is chosen such that the ingoing and outgoing principal null directions of the Kerr spacetime lie in the plane spanned by $\hat{e}_0$ and $\hat{e}_3$. For an observer with four-velocity $\hat{e}_0$ the vector $\hat{e}_0$ gives the spatial direction towards the center of the black hole [44].

We consider that light rays are issuing from the observer position into the past. The tangent vector for each light ray $\lambda(s)$ with coordinates $(r(s), \theta(s), \phi(s), t(s))$ can be written as

$$
\dot{\lambda} = \dot{r}\partial_r + \dot{\theta}\partial_\theta + \dot{\phi}\partial_\phi + \dot{t}\partial_t,
\tag{3.30}
$$
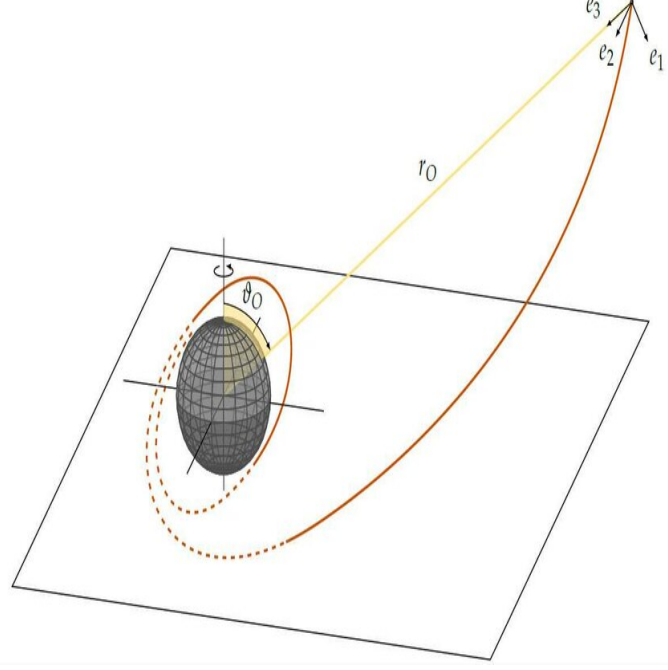
Figure 3.1. At an observation event with Boyer Lindquist coordinates (r_0, θ_0) we choose an orthonormal tetrad $(\hat{e}_0, \hat{e}_1, \hat{e}_2, \hat{e}_3)$ according to (3.29). For each light ray that is sent from the observation event into the past, the tangent vector can be written as a linear combination of $\hat{e}_0, \hat{e}_1, \hat{e}_2, \hat{e}_3$. In this way, we can assign celestial coordinates to the direction of the tangent vector.

where s is the arc length. However, the tangent vector at the observation event can be written as [44]

$$\dot{\lambda} = -\mathfrak{A}\hat{e}_0 + \mathfrak{B}\left(\sin\xi\cos\psi\hat{e}_1 + \sin\xi\sin\psi\hat{e}_2 + \cos\xi\hat{e}_3\right), \tag{3.31}$$

where $\mathfrak{A}$ and $\mathfrak{B}$ are positive factors. By (3.1), we have parameterized the light rays such that $g(\dot{\lambda}, \dot{\lambda}) = -\omega_{\mathrm{p}}^2$. Therefore, $\mathfrak{A}$ and $\mathfrak{B}$ must be related by using (3.31). We need to compute $g(\dot{\lambda}, \dot{\lambda})$,

$$g(\dot{\lambda}, \dot{\lambda}) = g\left(-\mathfrak{A}\hat{e}_0 + \mathfrak{B}\left(\sin\xi\cos\psi\,\hat{e}_1 + \sin\xi\sin\psi\,\hat{e}_2 + \cos\xi\,\hat{e}_3\right),\right.$$
$$\left.-\mathfrak{A}\hat{e}_0 + \mathfrak{B}\left(\sin\xi\cos\psi\,\hat{e}_1 + \sin\xi\sin\psi\,\hat{e}_2 + \cos\xi\,\hat{e}_3\right)\right), \tag{3.32}$$

As e_0, e_1, e_2, and e_3 are orthonormal, thus

$$g(\dot{\lambda}, \dot{\lambda}) = -\mathfrak{A}^2 + \mathfrak{B}^2,$$

41

After simplification, we get

$$\mathfrak{A}^2 - \mathfrak{B}^2 = \omega_{\text{p}}^2 \Big|_{(r_0, \theta_0)} . \tag{3.33}$$

The expression (3.31) describes the celestial coordinates ξ and ψ for the observer. ψ is azimuthal and ξ is colatitude angle. $\mathfrak{A}$ is determined for each light ray, computed as

$$\mathfrak{A} = g\left(\dot{\lambda}, e_0\right) = \frac{1}{\rho\sqrt{\Delta}} g\left(\dot{\lambda}, \left(r^2 + a^2\right) \frac{1}{c} \partial_{\text{t}} + a\partial_{\phi}\right),$$

$$= \frac{\left(r^2 + a^2\right)}{c\rho\sqrt{\Delta}} (-E) + \frac{a}{\rho\sqrt{\Delta}} (L_z),$$

$$= \frac{\left(r^2 + a^2\right)}{c\rho\sqrt{\Delta}} \left(\dot{t} g_{tt} + \dot{\phi} g_{\phi t}\right) + \frac{a}{\rho\sqrt{\Delta}} \left(\dot{t} g_{t\phi} + \dot{\phi} g_{\phi\phi}\right).$$

By using $E = c\omega_0$, $L_z = p_{\phi}$, we get

$$\mathfrak{A} = \frac{\left(r^2 + a^2\right)}{\rho\sqrt{\Delta}} \omega_0 + \frac{a}{\rho\sqrt{\Delta}} p_{\phi}. \tag{3.34}$$

From (3.33), we can find $\mathfrak{B}$

$$\mathfrak{A}^2 - \mathfrak{B}^2 = \omega_{\text{p}}^2 \Big|_{(r_0, \theta_0)} ,$$

Finally, we obtain

$$\mathfrak{B} = \sqrt{\frac{1}{\rho^2 \Delta} \left(\left(r^2 + a^2\right) \omega_0 + a p_{\phi}\right)^2 - \omega_{\text{p}}^2}, \tag{3.35}$$

where all equations are to be analyzed at (r_0, θ_0). To determine how the celestial coordinates ξ and ψ are related to the constants of motion $\mathcal{C}$ and p_{ϕ}, we compare the coefficients

42

of ∂_r in (3.30) and (3.31) leading to the result that

$$-\mathfrak{B}\cos\xi\frac{\sqrt{\Delta}}{\rho} = \dot{r}. \tag{3.36}$$

Squaring on both sides and then with the help of (3.17) and (3.35), we get

$$\left[\left(\left(r^2+a^2\right)\omega_0 + ap_\phi\right)^2 - \Delta\rho^2\omega_p^2\right]\left(1 - \sin^2\xi\right)$$
$$= -\left(\mathcal{C} + f_r(r)\right)\Delta + \left(\left(r^2+a^2\right)\omega_0 + ap_\phi\right)^2. \tag{3.37}$$

Solving for $\sin^2\xi$ and taking the square root (using $\sin\xi \geq 0$ as $0 \leq \xi \leq \pi$) yields

$$\sin\xi = \sqrt{\frac{\left(\mathcal{C} - f_\theta(\theta)\right)\Delta}{\left((r^2+a^2)\omega_0 + ap_\phi\right)^2 - \left(f_r(r) + f_\theta(\theta)\Delta\right)}}. \tag{3.38}$$

Similarly, we compare coefficients of ∂_ϕ in (3.30) and (3.31) which results in

$$-\frac{\mathfrak{A}a}{\rho\sqrt{\Delta}} - \frac{\mathfrak{B}\sin\xi\sin\psi}{\rho\sin\theta} = \dot{\phi} \tag{3.39}$$

Finally, by inserting equations (3.18),(3.34),(3.35) and (3.38) into (3.39), we get

$$\sin\psi = \left.\frac{-p_\phi - a\sin^2\theta\omega_0}{\sin\theta\sqrt{\mathcal{C} - f_\theta(\theta)}}\right|_{\theta_0}, \tag{3.40}$$

The shadow includes all points on the observer's sky, corresponding to tangent vectors of light rays that go to the horizon. The boundary points of the shadow spiral asymptotically towards spherical light rays and possess the same values for p_ϕ and $\mathcal{C}$ as these limiting spherical light rays.

By considering $a \neq 0$, we can use the values for p_ϕ and $\mathcal{C}$ from (3.25) and (3.26), where $r = r_p$ depicts the radius of the limiting spherical light rays. By inserting these expressions for $\mathcal{C}(r_p)$ and $p_\phi(r_p)$ into (3.38) and (3.40), we get the boundary of the shadow as a curve on the observer's sky, parameterized by r_p. It consists of two parts. The range $\psi = -\pi/2$

to $\pi/2$ corresponds to the lower part, while the range $\psi = \pi/2$ to $3\pi/2$ represents the upper part.

The parameter r_p ranges from a minimum value $r_{p,\min}$ to a maximum value $r_{p,\max}$ and back to $r_{p,\min}$. The values $r_{p,\min}$ and $r_{p,\max}$ are obtained by the condition that $\sin\psi = \pm 1$. Here we use the stereographic projection onto a plane that is tangent to the celestial sphere at the pole $\xi = 0$ and in this plane, Cartesian coordinates (dimensionless) are used, that is [34]

$$
\begin{aligned}
\mathrm{X}\left(r_p\right) &= -2\tan\left(\frac{\xi\left(r_p\right)}{2}\right)\sin\left(\psi\left(r_p\right)\right) \\
\mathrm{Y}\left(r_p\right) &= -2\tan\left(\frac{\xi\left(r_p\right)}{2}\right)\cos\left(\psi\left(r_p\right)\right)
\end{aligned}
\tag{3.41}
$$

In our plots, we use crosshairs to represent the Cartesian coordinate axes. Note that the pole $\xi = 0$, the origin of our Cartesian coordinate system corresponds to a past-directed ingoing principal null ray passing through the observer's position. This plotting technique, also utilized in reference [44], differs from the method proposed by Bardeen [45].

3.5.1 Plasma Distribution

Now, we are required to find out the plasma distributions that satisfy the separability condition in the HJ equation for further plotting the shadow. We take distributions that depict homogeneous and nonhomogeneous plasma around the black hole [34]. In this thesis, we primarily use the following distributions given below.

- **Case I**

In this case, we will consider the plasma distribution, given as

$$
f_{\mathrm{r}}(r) = \omega_{\mathrm{c}}^2 r^2 \quad f_\theta(\theta) = \omega_{\mathrm{c}}^2 a^2 \cos^2\theta
$$

such that $\omega_p^2(r, \theta) = \omega_c^2$ (ω_c= const.) that describes the homogeneous plasma distribution. In this case, we observe the shadow of the Kerr black hole in the presence of plasma just as in an environment without plasma. For this, we consider $f_r(r) = 0$, $\quad f_\theta(\theta) = 0$, then $\omega_p = 0$ implies to vacuum case. These conditions are qualitatively the same. We can see it in Fig. (3.2).
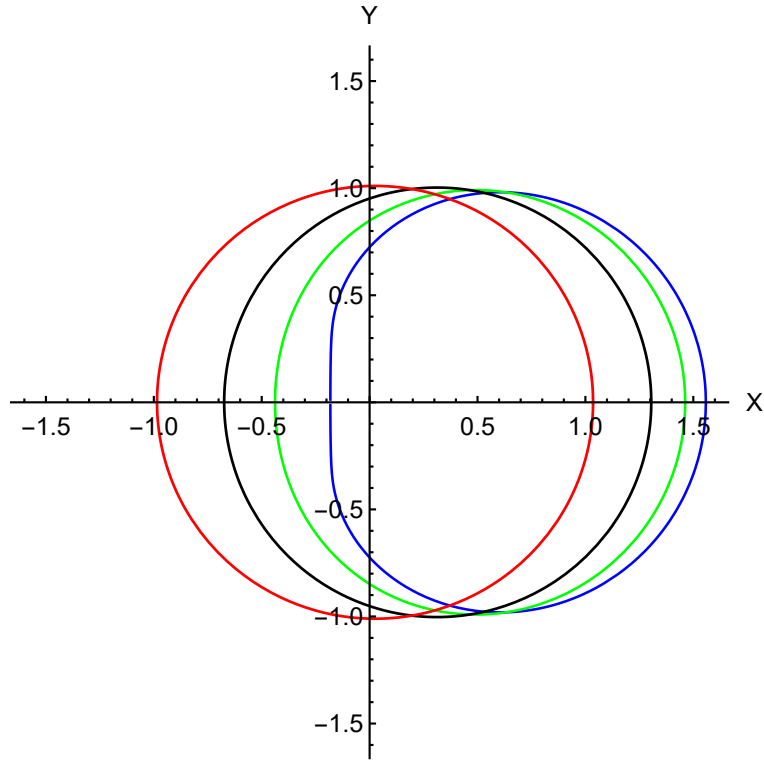
Figure 3.2. This figure shows the shadow for an observer $r_0 = 5m$ and $\theta_0 = \frac{\pi}{2}$ with the different spins $a = 0.04m$ (leftmost, red), $a = 0.5m$ (black), $a = 0.8m$ (green) and $a = 0.999m$ (blue). The axes labeled X and Y represent the Cartesian coordinates (3.41).

- **Case II**

In this case, we consider the plasma density with $f_r(r) = 0$ on Kerr spacetime, then we have

$$\omega_p(r, \theta)^2 = \frac{f_\theta(\theta)}{r^2 + a^2 \cos^2 \theta} \tag{3.42}$$

To satisfy inequality (3.4) we must have $f_\theta(\theta) \geq 0$. So we have opted for the $f_\theta(\theta) = \omega_c^2 m^2 (1 + 2\sin^2 \theta)$ where ω_c is constant with dimensions of frequency. This is the case

45

of nonhomogeneous plasma distribution. It can be seen the shadow in the absence of plasma shrunk as compared to the presence of plasma. We can see it in Fig. (3.2).
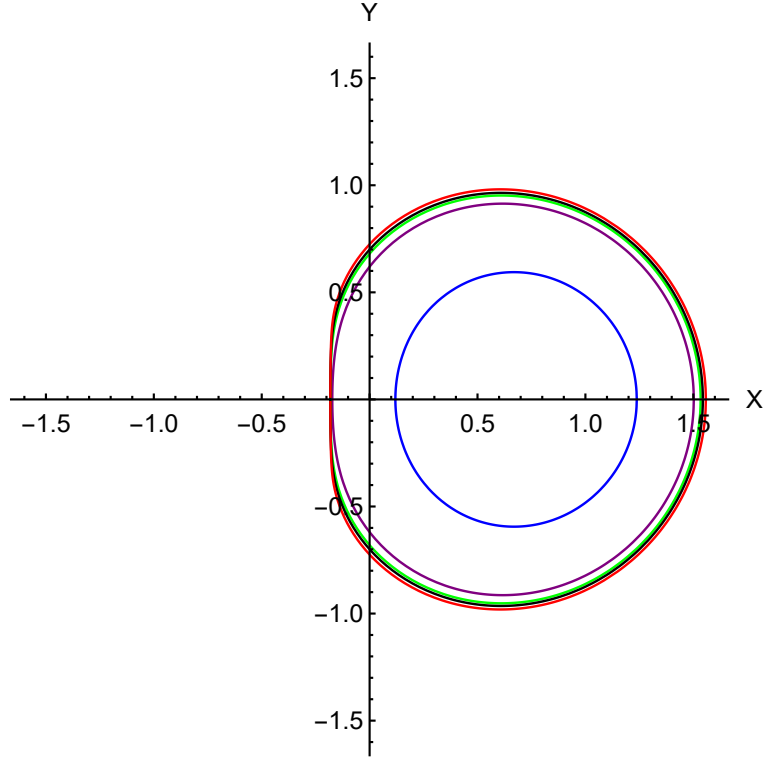
Figure 3.3. This figure shows the shadow for an observer at $r_0 = 5m$ and $\theta_0 = \frac{\pi}{2}$ with the spin $a = 0.999m$ and $\frac{\omega_c^2}{\omega_0^2}$ equal to 0 for (outermost,red); 1.9 (black); 2.5 (green); 3 (purple) and 7 (blue). When the forbidden region reaches the observer position the shadow has shrunk to a point.

- **Case III**

In this case, we consider the nonhomogeneous plasma such that $f_r(r) = \omega_c^2 \sqrt{m^3 r}$ and $f_\theta(\theta) = 0$. In this case, the choice of plasma density is motivated by power law density behaviors, such that plasma density is directly proportional to $r^{-3/2}$. In the vacuum case, all spherical light rays are unstable, and a forbidden region is formed when $\frac{\omega_c^2}{\omega_0^2}$ becomes bigger and the shadow disappears for all observers; see Fig. (3.3).

In this approach, the plasma only affects the trajectories of light rays, which changes the geometrical shape and size of the shadow. The size and shape of the shadow in the presence of plasma around a black hole differs based on the photon frequency compared to the vacuum case.
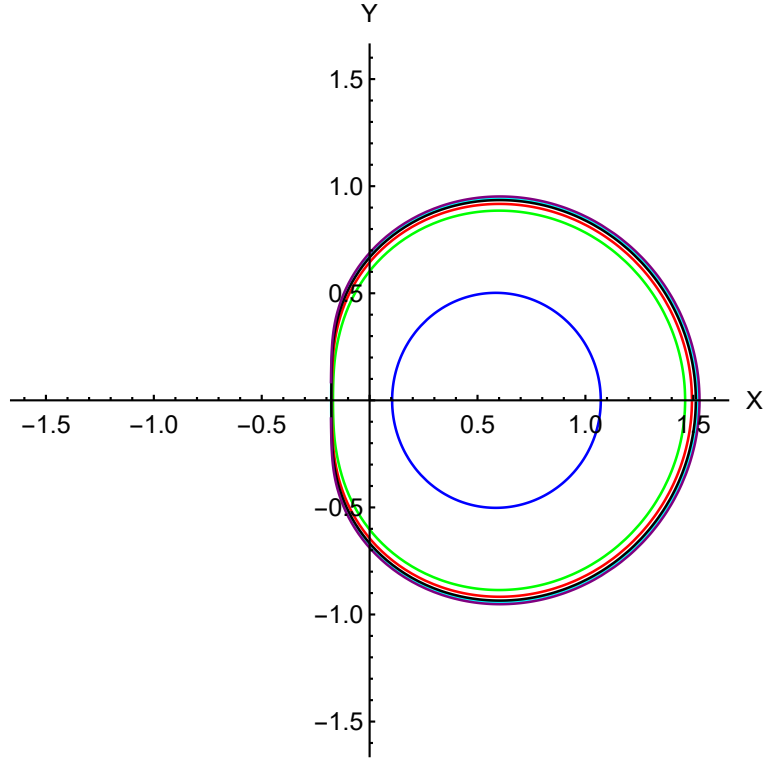
Figure 3.4. This figure displays the shadow for an observer at $r_0 = 5m$ and $\theta_0 = \frac{\pi}{2}$ with the spin $a = 0.999m$ and $\frac{\omega_c^2}{\omega_0^2}$ equal to 0 for (outermost,purple); 1.5 (black); 3.5 (Cyan); 9.2 (red); 12 (green) and 15.5 (blue). When the forbidden region reaches the equatorial plane the shadow has shrunk to a point.

The ratio of the plasma frequency to the photon frequency is the relevant quantity. The cases discussed above, conclude that the shadow is not much different from the vacuum case if the plasma frequency is small in comparison with the photon frequency. The properties of the shadow change drastically due to considerable changes in the photon regions if the plasma frequency is close to the photon frequency.

Across all applications in astrophysics, the difference between the vacuum case to the plasma case is important only for radio frequencies. An assessment of the effects in the case of Sgr A* and M87* can be seen in [46]. At low frequencies (large wavelengths), where the effects of the plasma are most important, scattering is predicted to be non-negligible. As scattering will partly diminish the shadow, it is anticipated that only at wavelengths of approximately 1 millimeter or below where the plasma effects are quite small, the shadow can be observed.

Chapter 4

Shadow of Kerr Black Hole in Modified Gravity(KMOG) in the Presence of Plasma and Naked Singularity

The mysteries of the universe have always been an interesting topic for physicists. Many cosmological observations specify that the universe is grappling with accelerated expansion, which is believed to be due to the existence of a mysterious form of energy named dark energy [47]. The matter that cannot be seen directly but can be observed by its gravitational effects on visible matter is known as dark matter (DM) [48]. This does not interact with the light and electromagnetic force. Modified gravity theories help to reveal the mysterious nature of DM and dark energy [49]. These theories are generated by modifying the matter or gravitational part of the Einstein–Hilbert action [50]

$$S_{EH} = \frac{1}{16\pi G} \int d^4x \sqrt{-g}\, R. \tag{4.1}$$

The modified theories with additional theories (vector, scalar) like scalar-tensor theories generalize GTR (tensor theory). The vector tensor theories are developed by adding a dynamical vector field coupled to gravity in the Einstein–Hilbert action. Moffat [51] devel-

oped a modified theory of gravity (MOG) termed scalar–tensor–vector gravity (STVG), which acts as an alternative to DM. This theory presents new fields in GTR, strengthening the gravitational field.
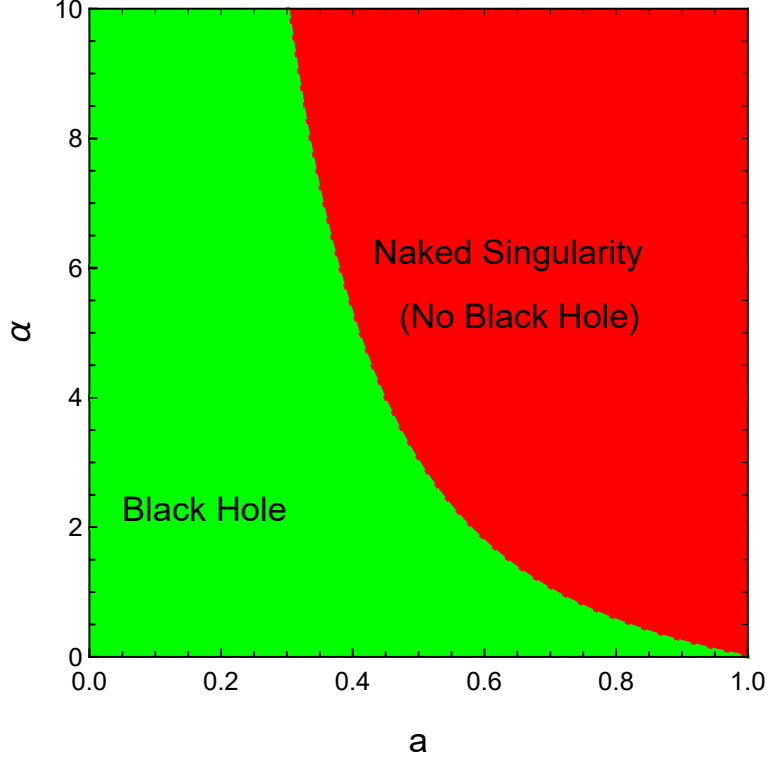
Figure 4.1. This plot shows the plane of deformation parameter α vs spin a of Kerr MOG black hole with $\mathcal{M} = 1$. The curve differs the black hole region with no black hole region.

4.1 Brief Introduction

The metric for rotating Kerr MOG black hole found by its angular momentum, mass, and a deformation parameter α in Boyer Lindquist coordinates is given by [51]

$$ds^2 = -\frac{\Delta - a^2 \sin^2 \theta}{\rho^2} dt^2 + \sin^2 \theta \left(\frac{\left(r^2 + a^2\right)^2 - \Delta a^2 \sin^2 \theta}{\rho^2} \right) d\phi^2$$
$$- 2a \sin^2 \theta \left(\frac{r^2 + a^2 - \Delta}{\rho^2} \right) dt d\phi + \frac{\rho^2}{\Delta} dr^2 + \rho^2 d\theta^2, \tag{4.2}$$

where

$$\Delta = r^2 - 2GMr + a^2 + \alpha G_{\mathrm{N}} G M^2, \quad \rho^2 = r^2 + a^2 \cos^2 \theta,$$

here, $G = G_N(1 + \alpha)$ is an enhanced gravitational constant with the contribution of Newton's gravitational constant G_N and the deformation rate α that is

$$\alpha = \frac{G - G_N}{G_N},$$

α is a dimensionless parameter and the modified charge parameter is

$$\mathcal{Q} = \sqrt{\alpha G_N} M. \tag{4.3}$$

For $\alpha = 0$, it will return toward the GTR and it would be a Kerr black hole metric, given above. Hence we can take α as the deviation parameter. The Newton mass M and the ADM mass $\mathcal{M}$ are related with

$$\mathcal{M} = (1 + \alpha)M. \tag{4.4}$$

Since Newton's mass (inertial mass) mainly causes the shadow, we will take Newton's mass as the unit. We can determine the black hole horizons by the roots of $\Delta = 0$, namely

$$r^2 - 2\mathcal{M}r + a^2 + \frac{\alpha}{1 + \alpha}\mathcal{M}^2 = 0. \tag{4.5}$$

After simplifying the equation above, it results in

$$r_{\pm} = G_N\mathcal{M} \pm \sqrt{\frac{G_N^2 \mathcal{M}^2}{1 + \alpha} - a^2}, \tag{4.6}$$

r_+ is termed the (outer) event horizon and r_- is called the (inner) Cauchy horizon. Note that $r_+ > r_-$. As mentioned above, when $\alpha = 0$, we acquire the horizon radii of the Kerr black hole. The black hole solution is present when $\frac{G_N^2 \mathcal{M}^2}{1+\alpha} > a^2$, and when $\frac{G_N^2 \mathcal{M}^2}{1+\alpha} < a^2$, we have the naked singularity. For simplicity, we will take $G_N = 1$ throughout this chapter.

50
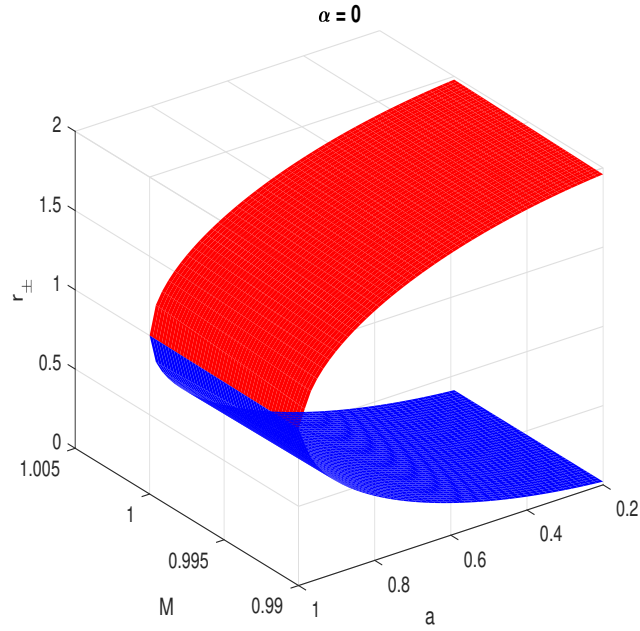
Figure 4.2. The figure implies the variation of $r_\pm$ with spin a and deformation parameter $\alpha = 0$ for Kerr black hole.
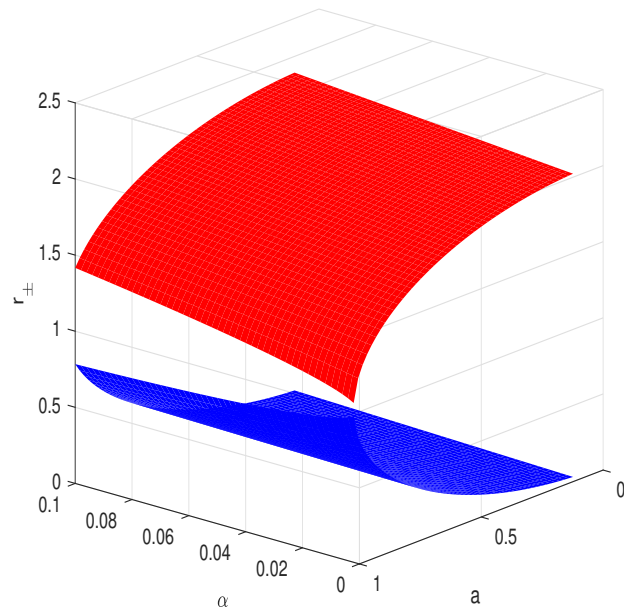
Figure 4.3. The figure implies the variation of $r_\pm$ with spin a and deformation parameter α for Kerr MOG black hole. We can observe that the presence of the deformation parameter deformed the shape of horizon radii.

Table 4.1. Corresponding to different values of the spin parameter a, the deformation parameter α range is shown for the Kerr MOG BH. Here the value of the mass parameter is $\mathcal{M} = 1$.

No.	a/M	Range of α
1	0.3	$0 \leq \alpha \leq 10.111$
2	0.4	$0 \leq \alpha \leq 5.250$
3	0.5	$0 \leq \alpha \leq 3.0$
4	0.6	$0 \leq \alpha \leq 1.777$
5	0.7	$0 \leq \alpha \leq 1.040$
6	0.8	$0 \leq \alpha \leq 0.562$
7	0.9	$0 \leq \alpha \leq 0.234$
8	0.99	$0 \leq \alpha \leq 0.020$
9	0.999	$0 \leq \alpha \leq 0.0020$
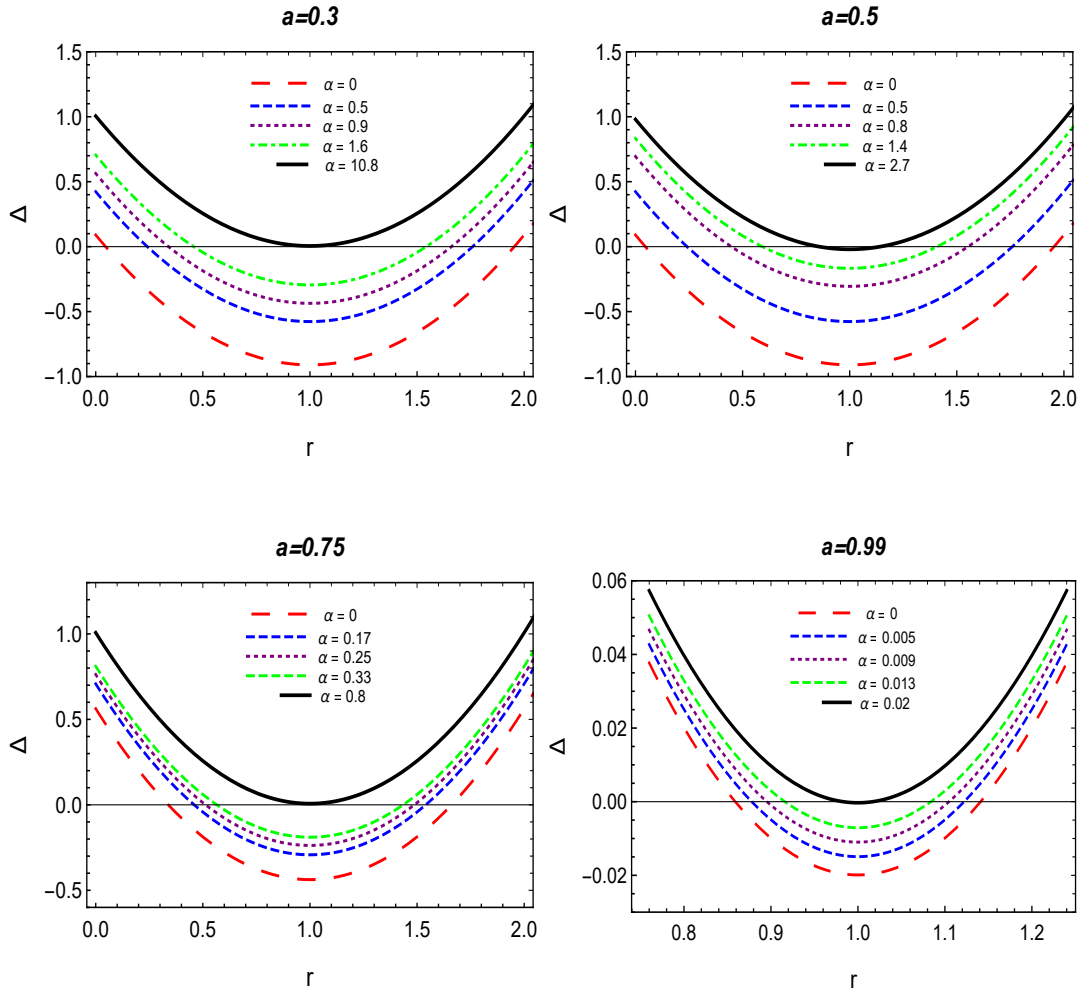
Figure 4.4. The following graphs represent behavior of event horizon ($\Delta = 0$) vs r for different values of MOG parameter. In the following plots dashed red lines correspond to the Kerr black hole with $\alpha = 0$ and black solid lines correspond to extremal Kerr MOG black hole. Here $\mathcal{M} = 1$.

The behavior of the event horizon is shown in Figs. (4.2), (4.3) and (4.4). It is obvious from the figures that there is a set of values for the parameters for which we have two horizons, such as the Cauchy horizon and the event horizon.

4.1.1 Refractive Index

Plasma is a dispersive medium corresponding to light propagation depending on the frequency. For a non-magnetized and pressureless plasma, the general form of the refractive index is given (3.3), where $x = x^\mu$, $\omega(x)$ is photon frequency and ω_p is plasma density (3.2). The photon frequency depends on the 4-velocity $\mathrm{U}^\mu(x)$. The frequency of the plasma is given by [52]

$$\hbar\omega(x) = p_\mu \mathrm{U}^\mu(x)$$

$$\mathrm{k}^\mu = p^\mu + p_\nu \mathrm{U}^\mu(x)\mathrm{U}^\nu(x) \tag{4.7}$$

where $\mathrm{k}^\mu(x)$ is a spatial vector depicting the wave number propagation vector. Its dispersion relation is

$$\hbar^2\omega^2(x) = \mathrm{k}^\mu(x)\mathrm{k}_\mu(x) + \hbar^2\omega_p^2(x) \tag{4.8}$$

as k^μ is a spatial vector, the corresponding propagation condition is provided in (3.4).

4.2 Hamiltonian Formulation

A Hamiltonian for light propagation in a non-magnetized pressureless plasma given in the above chapter (3.1) is

$$H(x, p) = \frac{1}{2}\left(g^{\mu\nu}(x)p_\mu p_\nu + \omega_{\mathrm{p}}(x)^2\right).$$

By using this, we obtain the Hamiltonian with MOG metric coefficients, which is expressed as follows:

$$H(x,p) = \frac{1}{2}\left[\frac{-1}{\Delta\rho^2}\left((r^2+a^2)^2 - \Delta a^2\sin^2\theta\right)p_t^2 + \frac{\Delta}{\rho^2}p_r^2 + \frac{1}{\rho^2}p_\theta^2 - \frac{2a(r^2+a^2-\Delta)}{\rho^2\Delta}p_t p_\phi\right.$$

$$\left. + \frac{\Delta - a^2\sin^2\theta}{\Delta\rho^2\sin^2\theta}p_\phi^2 + \omega_{\mathrm{p}}(r,\theta)^2\right],$$

$$= \frac{1}{2\rho^2}\left[\frac{-1}{\Delta}\left((r^2+a^2)p_t^2 + 2a(r^2+a^2)p_t p_\phi\right) + a^2\sin^2\theta p_t^2 + \Delta p_r^2 + p_\theta^2 + 2ap_t p_\phi\right.$$

$$\left. + \frac{p_\phi^2}{\sin^2\theta} - \frac{a^2}{\Delta}p_\phi^2 + \rho^2\omega_{\mathrm{p}}(r,\theta)^2\right],$$

The equation above leads to the following result

$$H = \frac{1}{2\rho^2}\left[\frac{-1}{\Delta}\left((r^2+a^2)p_t + ap_\phi\right)^2 + \left(a\sin\theta p_t + \frac{p_\phi}{\sin\theta}\right)^2 + \Delta p_r^2 + p_\theta^2 + \rho^2\omega_{\mathrm{p}}(r,\theta)^2\right].$$

(4.9)

4.3   Separation of Hamilton-Jacobi Equation for Light Rays in Plasma on Kerr MOG Spacetime

According to (4.9), the HJ equation is

$$0 = H\left(x, \frac{\partial S}{\partial x}\right)$$

(4.10)

$$p_\phi = \frac{\partial S}{\partial \phi}, \quad p_\theta = \frac{\partial S}{\partial \theta},$$

Using the expressions above, (4.10) transforms into the following

$$
0 = -\frac{1}{\Delta} \left(a \frac{\partial S}{\partial \phi} + \left(r^2 + a^2 \right) \frac{\partial S}{\partial t} \right)^2 + \left(\frac{1}{\sin \theta} \frac{\partial S}{\partial \phi} + \sin \theta \frac{\partial S}{\partial t} \right)^2
$$
$$
+ \left(\frac{\partial S}{\partial \theta} \right)^2 + \Delta \left(\frac{\partial S}{\partial r} \right)^2 + \rho^2 \omega_{\mathrm{p}}^2. \tag{4.11}
$$

With the separation ansatz given in (3.9) the HJ equation has the form of

$$
0 = -\frac{1}{\Delta} \left(a p_\phi + \left(r^2 + a^2 \right) \omega_0 \right)^2 + \left(\frac{p_\phi}{\sin \theta} + a \sin \theta \omega_0 \right)^2 + \Delta S_{\mathrm{r}}'(r)^2 + S_\theta'(\theta)^2
$$
$$
+ \omega_{\mathrm{p}}^2 \left(r^2 + a^2 \cos^2 \theta \right), \tag{4.12}
$$

where,

$$
p_\phi = \frac{\partial S}{\partial \phi}, \quad p_{\mathrm{t}} = \frac{\partial S}{\partial t} = \omega_0, \quad S_\theta'(\theta) = \frac{\partial S}{\partial \theta}, \quad S_{\mathrm{r}}'(r) = \frac{\partial S}{\partial r}.
$$

The separability of the HJ equation requires that, (3.10) must be arranged such that the right-hand side is independent of θ and the left-hand side is independent of r, as discussed in chapter 3. From (3.10) it can be seen that this is possible if and only if plasma frequency is of the form (3.11)

$$
\omega_{\mathrm{p}}(r, \theta)^2 = \frac{f_{\mathrm{r}}(r) + f_\theta(\theta)}{r^2 + a^2 \cos^2 \theta},
$$

with some function $f_{\mathrm{r}}(r)$ and $f_\theta(\theta)$. By putting (4.9) in (3.9), we get

$$
S_\theta'(\theta)^2 + \left(\frac{p_\phi}{\sin \theta} + a \sin \theta \omega_0 \right)^2 + f_\theta(\theta) =
$$
$$
-\Delta S_{\mathrm{r}}'(r)^2 + \frac{1}{\Delta} \left(a p_\phi + \left(r^2 + a^2 \right) \omega_0 \right)^2 - f_{\mathrm{r}}(r) = \mathcal{C}. \tag{4.13}
$$

The first expression is independent of r and the second one is independent of θ, with the Carter constant $\mathcal{C}$.

Thus, we have

$$p_\theta^2 = \mathcal{C} - \left(\frac{p_\phi}{\sin \theta} + a \sin \theta \omega_0 \right)^2 - f_\theta(\theta), \tag{4.14}$$

$$\Delta p_{\mathrm{r}}^2 = -\mathcal{C} + \frac{1}{\Delta} \left(\left(r^2 + a^2 \right) \omega_0 + a p_\phi \right)^2 - f_{\mathrm{r}}(r). \tag{4.15}$$

4.3.1 Equation of Motions for Light Rays in Plasma on Kerr MOG Spacetime

The equations of motion for light rays in a plasma within the Kerr MOG spacetime, derived using Hamilton's equations, are given as follows

$$\rho^4 \dot{\theta}^2 = \mathcal{C} - \left(\frac{p_\phi}{\sin \theta} + a \sin \theta \omega_0 \right)^2 - f_\theta(\theta), \tag{4.16}$$

$$\rho^4 \dot{r}^2 = \Delta \left(-\mathcal{C} + \frac{1}{\Delta} \left(\left(r^2 + a^2 \right) \omega_0 + a p_\phi \right)^2 - f_{\mathrm{r}}(r) \right) =: \mathcal{R}(r). \tag{4.17}$$

Now, we calculate the velocity components $\dot{t}$ and $\dot{\phi}$. By using (3.15)

$$\rho^2 \dot{t} = -\frac{1}{\Delta c} \left(\left(a p_\phi + \left(a^2 + r^2 \right) \frac{p_{\mathrm{t}}}{c} \right) + \left(a^2 + r^2 \right) \right) + 2 \left(\left(\frac{p_\phi}{\sin \theta} + \frac{a \sin \theta p_{\mathrm{t}}}{c} \right) \frac{a \sin \theta}{c} \right)$$

This ultimately results in the following form

$$\rho^2 \dot{t} = \frac{1}{\Delta} \left[\left((r^2 + a^2)\rho^2 + 2\mathcal{M}ra^2 \sin^2 \theta - \frac{\alpha}{(1+\alpha)} \mathcal{M}^2 a^2 \sin^2 \theta \right) \omega_0 - \left(2\mathcal{M}r - \frac{\alpha}{1+\alpha} \mathcal{M}^2 \right) a p_\phi \right].$$

Next, we take (3.15) and solve it to find $\dot{\phi}$

$$\rho^2 \dot{\phi} = -\frac{1}{\Delta} \left(a p_\phi + \left(r^2 + a^2 \right) \omega_0 \right) + \frac{p_\phi + a \sin^2 \theta \omega_0}{\sin^2 \theta},$$

The resulting expression is given by

$$\rho^2 \dot{\phi} = \frac{1}{\Delta \sin^2 \theta} \left[-\left(2\mathcal{M}ra\sin^2\theta - \frac{\alpha}{(1+\alpha)}\mathcal{M}^2 a \sin^2\theta \right)\omega_0 + \left(\rho^2 - 2\mathcal{M}r + \frac{\alpha}{(1+\alpha)}\mathcal{M}^2 \right)p_\phi \right].$$

(4.18)

4.3.2 Photon Region

By using (4.15) and taking its derivative w.r.t r, we get

$$0 = \mathcal{R}'(r) = -(\mathcal{C} + f_r(r))2(r - \mathcal{M}) - f_r'(r)\Delta + 4rp_t \left((r^2 + a^2)\omega_0 + ap_\phi \right). \quad (4.19)$$

We will now calculate the constant of motions $\mathcal{C}$ and ap_ϕ by using (3.15) and (4.15). We get the value ap_ϕ after solving the (3.17) as follows

$$ap_\phi = \frac{\omega_0}{r - \mathbf{M}} \left(\left(a^2 - r^2 + \frac{\alpha}{1+\alpha}\mathcal{M}r \right)\mathcal{M} \pm \Delta r \sqrt{1 - \frac{f'(r)(r - \mathcal{M})}{2r^2\omega_0^2}} \right)$$

The resulting equation for ap_ϕ takes the form

$$ap_\phi = \frac{\omega_0}{r - \mathcal{M}} \left(\left(a^2 - r^2 + \frac{\alpha}{1+\alpha}\mathcal{M}r \right)(\mathcal{M}) \pm \Delta r \sqrt{1 - \frac{f'(r)(r - \mathcal{M})}{2r^2\omega_0^2}} \right). \quad (4.20)$$

Similarly, we obtain the value of $\mathcal{C}$ is given by

$$\mathcal{C} = \frac{\omega_0^2 r^2 \Delta}{(r - \mathcal{M})^2} \left(1 \pm \sqrt{1 - \frac{f'(r)(r - \mathcal{M})}{2r^2\omega_0^2}} \right)^2 - f_r(r),$$

$$\mathcal{C} = \frac{\omega_0^2 r^2 \Delta}{(r - \mathcal{M})^2} \left(1 \pm \sqrt{1 - \frac{f'(r)(r - \mathcal{M})}{2r^2\omega_0^2}} \right)^2 - f_r(r). \quad (4.21)$$

57

As the left-hand side of (4.16) is the square of a real quantity, the right-hand side must be non-negative. From (4.16), we find that

$$0 \leq \mathcal{C} - \left(\frac{p_\phi}{\sin \theta} + a \sin \theta \omega_0 \right)^2 - f_\theta(\theta),$$

$$\left(\mathcal{C} - f_\theta(\theta) \right) \sin \theta \geq \left(p_\phi + a \sin^2 \theta \omega_0 \right)^2. \tag{4.22}$$

Inserting (4.20)) and (4.21) into the above equation, gives photon region as follows

$$\left(\frac{r^2 \Delta}{(r - \mathcal{M})^2} \left(1 \pm \sqrt{1 - f_r'(r) \frac{(r - \mathcal{M})}{2 r^2 \omega_0^2}} \right)^2 - \frac{f_r(r) + f_\theta(\theta)}{\omega_0^2} \right) a^2 \sin^2 \theta \geq$$

$$\left(\frac{1}{(r - \mathcal{M})} \left(\mathcal{M} \left(a^2 - r^2 \right) \pm r \Delta \sqrt{1 - f_r'(r) \frac{(r - \mathcal{M})}{2 r^2 \omega_0^2}} \right) + a^2 \sin^2 \theta \right)^2.$$

4.4 Calculation of Shadow of Kerr MOG Black Hole in the Presence of Plasma

We select an orthonormal tetrad as (3.29). This tetrad is orthonormal and well-defined for any observer position in the domain of outer communication. The timelike vector $\hat{e}_0$ is to be interpreted as the four-velocity of our observer. It is selected so that the ongoing and outgoing principal null directions of the Kerr MOG spacetime are in the plane spanned by $\hat{e}_0$ and $\hat{e}_3$. For an observer with four-velocity $\hat{e}_0$ the vector $\hat{e}_0$ gives the spatial direction towards the center of the black hole [44].

The tangent vector for each light ray $\lambda(s)$ with coordinates $(r(s), \theta(s), \phi(s), t(s))$ can be written as[34]

$$\dot{\lambda} = \dot{r} \partial_r + \dot{\theta} \partial_\theta + \dot{\phi} \partial_\phi + \dot{t} \partial_t, \tag{4.23}$$

However, the tangent vector at the observation event can be written as

$$\dot{\lambda} = -\mathfrak{A}\hat{e}_0 + \mathfrak{B}\left(\sin\xi\cos\psi e_1 + \sin\xi\sin\psi\hat{e}_2 + \cos\xi\hat{e}_3\right). \qquad (4.24)$$

Here, the above expression describes the celestial coordinates ξ and ψ for the observer. ψ is azimuthal and ξ is colatitude angle as discussed in chapter 3. $\mathfrak{A}$ determined for each light ray is

$$\mathfrak{A} = \frac{(r^2 + a^2)}{\rho\sqrt{\Delta}}\omega_0 + \frac{a}{\rho\sqrt{\Delta}}p_\phi. \qquad (4.25)$$

The expression for $\mathfrak{B}$ can be obtained from (3.33), as shown below

$$\mathfrak{B} = \sqrt{\frac{1}{\rho^2\Delta}\left((r^2 + a^2)\omega_0 + ap_\phi\right)^2 - \omega_{\mathrm{p}}^2}. \qquad (4.26)$$

To examine the relationship between the celestial coordinates ξ and ψ and the constant of motion $\mathcal{C}$ and p_ϕ, we analyze equations (3.34) and (3.35), leading to the following

$$\sin\xi = \sqrt{\left.\frac{\left(\mathcal{C} - f_\theta(\theta)\right)\Delta}{\left((r^2 + a^2)\omega_0 + ap_\phi\right)^2 - \left(f_{\mathrm{r}}(r) + f_\theta(\theta)\Delta\right)}\right|_{(r_0,\theta_0)}} \qquad (4.27)$$

$$\sin\psi = \left.\frac{-p_\phi - a\sin^2\theta\omega_0}{\sin\theta\sqrt{\mathcal{C} - f_\theta(\theta)}}\right|_{(r_0,\theta_0)}. \qquad (4.28)$$

The shadow includes all points on the observer's sky, corresponding to tangent vectors of light rays that go to the horizon. The boundary points of the shadow spiral asymptotically towards spherical light rays and possess the same values for p_ϕ and $\mathcal{C}$ as these limiting spherical light rays. Here, we use stereographic projection onto a plane tangent to the celestial sphere at the pole where $\xi = 0$. We employ dimensionless Cartesian coordinates in this plane, as given in (3.41). We will now discuss some cases that depict the shadows cast by a Kerr MOG black hole, considering the plasma effects as well as the deformation parameter related to modified gravity α.

Case I: In this, we observed the shadow of the Kerr MOG black hole in the vacuum such as we consider $\omega_p = 0$. In this case, we observe the shadow of the Kerr MOG black hole in an environment without plasma. For this, we consider $f_r(r) = 0$, $f_\theta(\theta) = 0$. The plasma distribution $f_r(r) = \omega_c^2 r^2$ and $f_\theta(\theta) = \omega_c^2 a^2 \cos^2\theta$ such that $\omega_p^2(r,\theta) = \omega_c^2$ (ω_c= const.) that describes the homogeneous plasma distribution, these conditions are qualitatively the same as discussed above. As we can see it in Fig. (4.5). **Case II**: Secondly, we observe the shadow of Kerr MOG black hole behavior in the presence of an inhomogeneous plasma environment. Here we choose $f_r(r) = 0$ and $f_\theta(\theta) = \omega_c^2 \mathcal{M}^2(1 + 2\sin^2\theta)$ where ω_c is constant with dimensions of frequency [34]

$$\omega_p(r,\theta) = \frac{\omega_c^2 \mathcal{M}^2(1 + 2\sin^2\theta)}{(1+\alpha)^2(r^2 + a^2\cos^2\theta)}. \tag{4.29}$$

We must have $f_\theta(\theta) \geq 0$ to satisfy the inequality (3.4). The main finding is that the shadow for a homogeneous plasma environment is bigger than the inhomogeneous one.
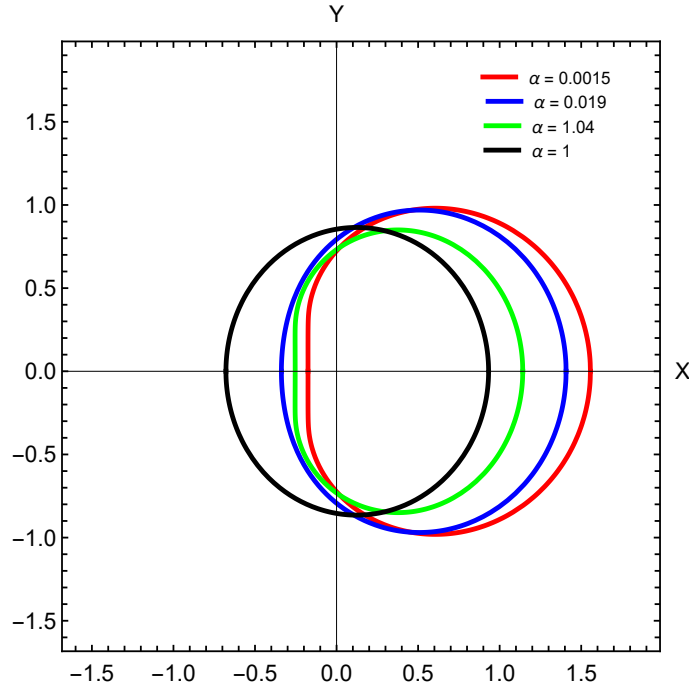
Figure 4.5. This figure depicts shadow for an observer at $r_0 = 5$ and $\theta_0 = \frac{\pi}{2}$ with different spins $a = 0.04$ (leftmost, black), $a = 0.7$ (green), $a = 0.9$ (blue) and $a = 0.999$ (red) and deformation parameter α .The axes labeled X and Y represent the Cartesian coordinates (3.41).

60

Case III: In the next case, we consider nonhomogeneous plasma where plasma density posses $f_r(r) \propto \sqrt{r}$ and $f_\theta(\theta) = 0$ in Kerr MOG spacetime. We assumed θ dependence in addition, to satisfy the separability condition, we have

$$\omega_p(r,\theta)^2 = \frac{\omega_c^2 \sqrt{\mathcal{M}^3 r}}{(1+\alpha)^{\frac{3}{2}}(r^2 + a^2 \cos^2\theta)} \qquad (4.30)$$

where ω_c is constant with dimensions of frequency. The shadow vanishes for observer if $\frac{\omega_c^2}{\omega_0^2}$ becomes too large.
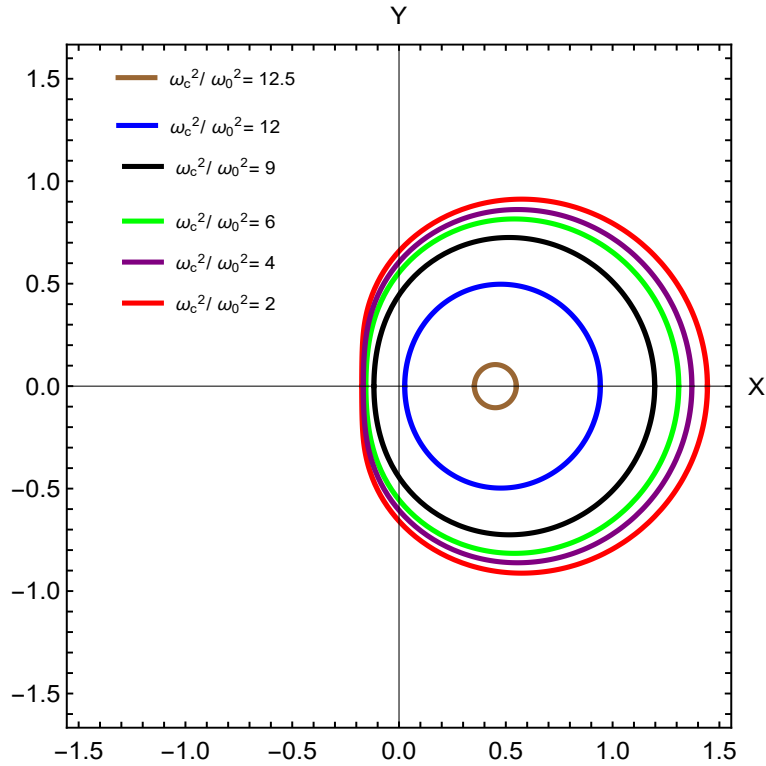
Figure 4.6. This figure shows the shadow for an observer at $r_0 = 5$ and $\theta_0 = \frac{\pi}{2}$ with the spin $a = 0.999$ and deformation parameter $\alpha = 0.0020$. When the forbidden region reaches the observer position the shadow has shrunk to a point.

In Fig. (4.5) we use different values of α with spin a accordingly and we can observe that the shadow does not differ for Kerr MOG black hole [53] for the vacuum case. In Fig. (4.6), the shadow becomes invisible for certain plasma frequencies, leaving a completely illuminated sky. By examining the photon region, it is observed that a specific critical frequency ratio, $\frac{\omega_c^2}{\omega_0^2}$, exists. Beyond this threshold, a forbidden zone appears where the

propagation condition (3.4) is no longer met. As the plasma frequency increases, the forbidden region expands until it fully encloses the black hole.

Low-energy photons are unable to pass through this forbidden zone and are deflected. Consequently, observers near the equatorial plane ($\theta_0 = \pi/2$) will no longer observe the shadow first. For those situated beyond the forbidden region, the sky will appear entirely bright, while it will remain completely dark for observers between the forbidden region and the black hole.
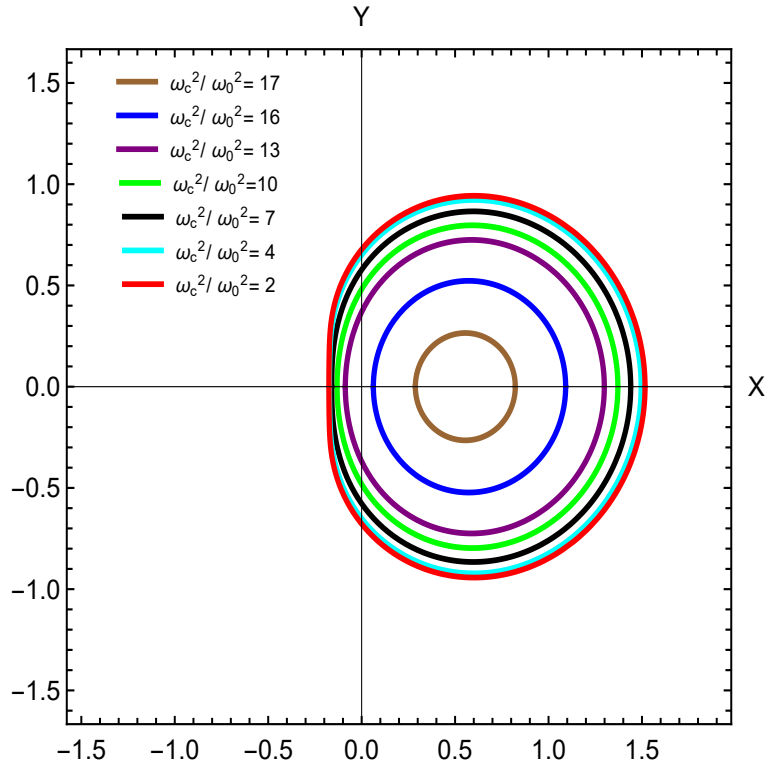
Figure 4.7. This figure shows the shadow for an observer at $r_0 = 5$ and $\theta_0 = \frac{\pi}{2}$ with the spin $a = 0.999$ and deformation parameter $\alpha = 0.0020$. At $\frac{\omega_c^2}{\omega_0^2} \approx 17.45$ it has vanished.

By increasing the ratio $\frac{\omega_c^2}{\omega_0^2}$ expands the forbidden region until it entirely encloses the black hole at a critical value, $\frac{\omega_c^2}{\omega_0^2}$. At this point, the shadow vanishes for all observers, leading to a completely bright sky, as in Fig. (4.7) with $\frac{\omega_c^2}{\omega_0^2} \approx 17.45$ shadow vanishes. As previously observed, the ratio $\frac{\omega_c^2}{\omega_0^2}$ depends on the metric model. However, in this case, it also varies with the MOG parameter α. As the values of spin parameter are increased

within the deformation parameter α, the ratio $\frac{\omega_c^2}{\omega_0^2}$ also increases. With the increase in plasma frequency, the effects of the plasma become more significant, counteracting the gravitational effects [52]. This occurs because, for over-dense plasma distributions, the plasma behaves as a repulsive medium, unlike the attractive nature of the gravitational field. Consequently, the shadow shrinks as the plasma frequency rises.

Shadow of KMOG Naked Singularity

In this section, we analyze the shadow of Kerr MOG singularities. We discuss the causal structure and some of the geometrical properties of naked singularities on Kerr MOG spacetime and the results are compared to those of Kerr naked singularities when deformation parameter $\alpha = 0$. In the case of Kerr MOG naked singularity, the photon sphere exists only for retrograde photon orbits, whereas for a Kerr MOG black hole, the photon sphere exists for both prograde and retrograde photon orbits. Consequently, the naked singularity projects an arc-shaped shadow.

4.5 Analytical Shadow of KMOG Naked Singularity

A massive, rotating naked singularity can be attained from the Kerr MOG metric in the Boyer Lindquist coordinates (t, r, θ, ϕ) given by (4.2).

For $a = \frac{a}{G_{\mathcal{N}}\mathcal{M}} > 1$, it is referred to a Kerr naked singularity while for $a = \frac{a}{G_{\mathcal{N}}\mathcal{M}} < 1$ there exists black hole solution. When $a = \frac{a}{G_{\mathcal{N}}\mathcal{M}} = 1$, it is said to be an extremal black hole solution. Meanwhile, for the Kerr MOG black hole, these limits can be simplified in the following way, if we take $\alpha = 1$ then these limits are described as $a > \frac{1}{\sqrt{2}}$ for Kerr MOG naked singularity situation and $a < \frac{1}{\sqrt{2}}$ for Kerr MOG black hole solution and for $a = \frac{1}{\sqrt{2}}$, it is extremal limit. Similarly, these limits are also found with $\alpha = 2$ [29].

Table 4.2. Corresponding to different values of the spin parameter a, the deformation parameter α range is shown for the Kerr MOG naked singularity. Here the value of the mass parameter is $\mathcal{M} = 1$.

No.	$a/\mathcal{M}$	Range of α
1	1.1	$\alpha > -0.17355$
2	1.2	$\alpha > -0.30555$
3	1.3	$\alpha > -0.40828$
4	1.4	$\alpha > -0.48979$
5	1.5	$\alpha > -0.55556$
6	1.6	$\alpha > -0.609375$
7	1.7	$\alpha > -0.653979$
8	1.8	$\alpha > -0.691358$
9	1.9	$\alpha > -0.722991$

4.5.1 Unstable spherical Photon Orbits around KMNs

There are two Killing vectors given in section (2.1.1.1) demonstrating the time and azimuthal translation. Conserved quantities can be obtained from the symmetries of the physical laws.

By projecting the Killing vectors along the covariant four-momentum vector p_μ, we find conserved energy E and conserved angular momentum in the ϕ direction L_z that is given in (2.2). To examine the spherical photon orbits and the shadow of Kerr MOG naked singularity we use the HJ equation (2.3) as discussed above. The solution to (2.3) can be separated into different components depending on each coordinate, we use ansatz (2.4). The resulting equation is

$$H = \frac{1}{2} \left(\frac{-1}{\Delta \rho^2} \left((r^2 + a^2)^2 - a^2 \sin^2 \theta \Delta \right) p_t^2 + \frac{\Delta}{\rho^2} S_r'(r)^2 + \frac{1}{\rho^2} S_\theta'(\theta)^2 - \frac{4Mar}{\rho^2 \Delta} p_t p_\phi \right.$$
$$\left. + \frac{\Delta - a^2 \sin^2 \theta}{\Delta \rho^2 \sin^2 \theta} p_\phi^2 \right). \tag{4.31}$$

Now, using (2.4) and (4.31), we obtain the equations of motion for null geodesics for each of the coordinates as follows

$$\rho^2 \Delta \dot{t} = \Xi E - a(r^2 + a^2 - \Delta)L_z,$$

$$\rho^2 \Delta \dot{t} = \Xi E - a(2\mathcal{M}r - \frac{\alpha}{1+\alpha}\mathcal{M}^2)L_z, \tag{4.32}$$

where, $\Xi = (a^2 + r^2)^2 - \Delta a^2 \sin^2\theta$ and $\dot{\phi}$ takes the following form with the deformation parameter α

$$\rho^2 \Delta \dot{\phi} = (r^2 + a^2 - \Delta)E + (\rho^2 - 2\mathcal{M}r + \frac{\alpha}{1+\alpha}\mathcal{M}^2)\frac{L_z}{\sin^2\theta}$$

$$\rho^2 \Delta \dot{\phi} = a(2\mathcal{M}r - \frac{\alpha}{1+\alpha}\mathcal{M}^2)E + (\rho^2 - 2\mathcal{M}r + \frac{\alpha}{1+\alpha}\mathcal{M}^2)L_z \csc^2\theta, \tag{4.33}$$

Similarly, we proceed for $\dot{\theta}$ and $\dot{r}$, given as

$$\rho^4 \dot{\theta}^2 = \mathcal{C} - \left(\frac{L_z^2}{\sin^2\theta} - E^2 a^2\right)\cos^2\theta, \tag{4.34}$$

$$\rho^4 \dot{r}^2 = -\mathcal{C}\Delta + (r^2 + a^2)E^2 - 2a(r^2 + a^2 - \Delta)EL_z + a^2 L_z^2 - a^2 E^2 \Delta - L_z^2 \Delta \tag{4.35}$$

The radial equation of motion (4.35) can be rewritten in terms of effective potential $\mathcal{R}(r)$ is

$$\left(\frac{\rho^2}{E}\right)^2 \dot{r}^2 = -\frac{\Delta\mathcal{C}}{E^2} + (r^2 + a^2)^2 - 2a(r^2 + a^2 - \Delta)\frac{L_z}{E} + a^2\frac{L_z}{E^2} - a^2\Delta - \left(\frac{L_z^2}{E}\right)^2 \Delta,$$

$$\left(\frac{\rho^2}{E}\right)^2 \dot{r}^2 = -\Delta\zeta + (r^2 + a^2)^2 - 2a(r^2 + a^2 - \Delta)\varphi + a^2\varphi^2 - a^2\Delta - \varphi^2\Delta. \tag{4.36}$$

Here, we define the impact parameters as $\varphi = \frac{L_z}{E}$ and $\zeta = \frac{\mathcal{C}}{E^2}$, where $\mathcal{C}$ is Carter's constant, representing a third conserved quantity that arises from the separability of the

65

HJ equation. $\mathcal{C}$ is related to geodesics in the latitudinal direction. Now, the effective potential derived from the radial equation of motion is as follows

$$\mathcal{R}(r) = -\Delta\zeta + (r^2 + a^2)^2 - 2a(r^2 + a^2 - \Delta)\varphi + a^2\varphi^2 - a^2\Delta - \varphi^2\Delta. \qquad (4.37)$$

4.5.2 Spherical Photon Orbits and Shadow

We obtain two sets of solutions by solving the following conditions for spherical photon orbits with constant radius $r = r_{\rm p}$, given as

$$\mathcal{R}(r) = 0 \quad \text{and} \quad \frac{d}{dr}\mathcal{R}(r) = 0 \qquad (4.38)$$

However, only one of these solutions is physically meaningful and applies to our calculations.

$$\varphi = \frac{a^2\mathcal{M} + a^2 r_{\rm p} - 3\mathcal{M}r_{\rm p}^2 + r_{\rm p}^3 + a^2\mathcal{M}\alpha}{a(\mathcal{M} - r_{\rm p})(1 + \alpha)}$$
$$+ \frac{a^2 r_{\rm p}\alpha + 2\mathcal{M}^2 r_{\rm p}\alpha - 3\mathcal{M}r_{\rm p}^2\alpha + r_{\rm p}^3\alpha)}{a(\mathcal{M} - r_{\rm p})(1 + \alpha)} \qquad (4.39)$$

$$\zeta = \frac{r_{\rm p}}{-a^2\mathcal{M} + a^2 r_{\rm p} - a^2\mathcal{M}\alpha + r_{\rm p}a^2\alpha}\left(\frac{-4a^2\mathcal{M}(1+\alpha)\left(r_{\rm p} - \mathcal{M}\alpha + r_{\rm p}\alpha\right)}{a(\mathcal{M} - r_{\rm p})(1+\alpha)}\right.$$
$$\left. + \frac{\left(2\mathcal{M}^2\alpha + \alpha\mathcal{M}^2 - 3\mathcal{M}\left(r_{\rm p}(1+\alpha) + r_{\rm p}^2(1+\alpha)\right)\right)^2}{a(\mathcal{M} - r_{\rm p})(1+\alpha)}\right) \qquad (4.40)$$

At the equatorial plane, since $\zeta = 0$, so the critical orbits of the photon $(r_{\rm ph})$ can be determined by the roots of (4.40) in Kerr MOG naked singularity spacetime. As discussed, the impact parameters φ and ζ are significant in finding the shape of the shadow. We can find stable and unstable photon orbits around the Kerr MOG naked singularity as before for Kerr naked singularity. In the context of Kerr MOG naked singularity, a single photon sphere for retrograde motion presents a specific critical impact parameter that describes

the boundary between captured light and light that is escaped by the singularity that we can see in Fig. (4.7) and Fig. (4.8).

This figure presents the behavior of φ and ζ as a function of r, where we take $a = 1.38$, $M = 1$, and $\alpha = -0.4749$. Orbits with a positive φ value depict the prograde equatorial motion of photons, and those with a negative φ value describe the retrograde equatorial orbit. For Kerr MOG naked singularity, ζ_{KMNs} disappears at $r_{\text{ph}} = 2.98$ as presented in Fig. (2.4). Corresponding to this radius the circular orbit is retrograde, since φ_{KMNs} is negative at $r_{\text{ph}} = 2.98$, and we identify that for the prograde equatorial motion of photons, no photon sphere exists. Hence, the corresponding critical impact parameter is $\varphi_{\text{KMNs}} = 7.68$, there is only one photon sphere $r_{\text{ph}} = 2.98$ for the retrograde motion of null geodesics in Kerr MOG naked singularity spacetime. For Kerr MOG naked singularity, the prograde equatorial orbit does not exist. The retrograde equatorial orbit separates between orbits that terminate at the singularity and those that diminish to infinity. Off the equatorial plane, all orbits that approach the Kerr MOG naked singularity can escape or unbound.
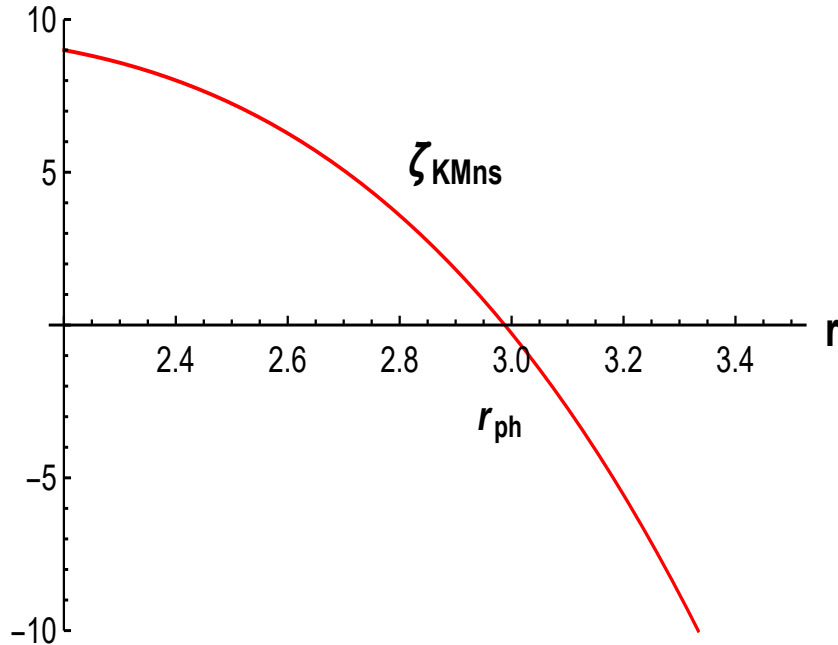
Figure 4.8. This figure demonstrates the behavior of ζ for the Kerr MOG naked singularity as a function of radial coordinate r. Here, we take $a = 1.38$, $\mathcal{M} = 1$ and $\alpha = -0.04749$.
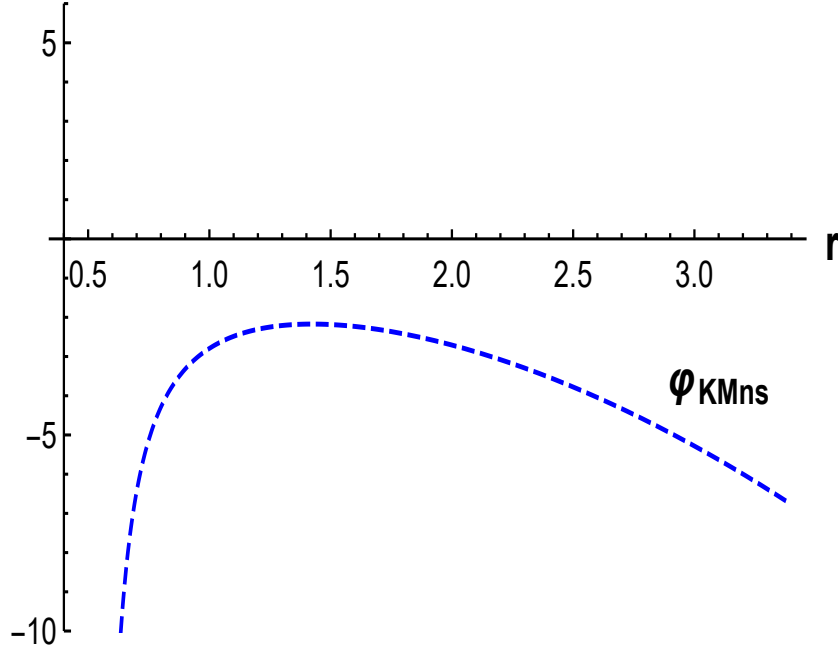
Figure 4.9. This figure depicts the behavior of φ for the Kerr MOG naked singularity as a function of radial coordinate r. Here, we take $a = 1.38$, $\mathcal{M} = 1$ and $\alpha = -0.04749$.

Unstable photon orbits surrounding Kerr MOG naked singularity exist in the range $r_{ms} < r_{\mathrm{p}} < r_{ph}$ where r_{ms} is a marginally stable radius and r_{ph} is the equatorial retrograde circular radius that we can get numerically by putting $\zeta = 0$ also can be seen in Fig.(4.7). The marginally stable radius r_{ms} can be calculated by

$$\frac{d^2}{dr^2}\mathcal{R}(r) = 0, \tag{4.41}$$

Which yields,

$$r_{\mathrm{ms}} = \frac{\mathcal{M} + \mathcal{M}\alpha}{1 + \alpha} + \frac{\left(a^2\mathcal{M} - \mathcal{M}^3 + 3a^2\mathcal{M}\alpha - 2\mathcal{M}^3\alpha + 3a^2\mathcal{M}\alpha^2 - a^2\mathcal{M}\alpha^3\right)^{\frac{1}{3}}}{1 + \alpha}. \tag{4.42}$$

While stable photon orbits with $r < r_{ms}$ are normally concealed inside the event horizon for the Kerr black hole, they have physical importance for Kerr naked singularity because of the absence of an event horizon. However, bounded photon orbits cannot be observed by distant observers, so they are unrelated to our study of the observational aspects of Kerr naked singularity [38] and follow the same for Kerr MOG naked singularity.

We can obtain the apparent shape of the shadow seen by the asymptotic observer if we consider the celestial coordinates σ and τ, which are the coordinates of the asymptotic observer's sky. The general expression to find celestial coordinates σ and τ by (2.27) and (2.28). Figures (4.10) to (4.12) depict the analytical shadow of Kerr MOG naked singularity with different values of spin parameter a, deformation parameter α inclination angle i, by casting the unstable photon orbits to an image plane at infinity with orthogonal coordinates σ and τ.

In Fig. (4.10) with the different values of MOG parameter α, we get the different behavior of shadow of Kerr MOG naked singularity, considering the negative values of α which meets the criteria of inequality, we get the shadow of Kerr MOG is lesser than Kerr naked singularity ($\alpha = 0$). While taking into account the positive values of α that correspond to marginally stable radius r_{ms} after that value of α, the real values of r_{ms} will not be obtained by using (4.42). Consequently, these values outline the range of α for plotting the shadow of Kerr MOG naked singularity. In Fig. (4.11) we can discern that by increasing the spin a, the shadow pattern concerning the negative values of α becomes smaller. Similarly in Fig. (4.12), we can observe that the shadow at negative values of α differs significantly from that at positive values of α [28]. The shadow increases in size when it takes on positive values and becomes a closed for the spin value $a = 2$

4.5.3   Toplogical Aspects of Kerr MOG Naked Singularity Shadow

The shadow of a Kerr MOG black hole consistently exhibits a closed geometry. In contrast, the shadow of a Kerr MOG naked singularity may display a gap due to the absence of a prograde equatorial circular orbit. Additionally, the shadow is symmetric concerning the σ-axis on the image plane. The interaction between the photon sphere radius (r_{ph}) and the radius of the marginally stable orbit (r_{ms}) plays a key role in determining the shadow features of Kerr and Kerr MOG naked singularities. Analyzing how changes in these radii impact the shadow's geometry and characteristics is essential for differentiating naked singularities from black holes and for investigating the consequences of cosmic

censorship.
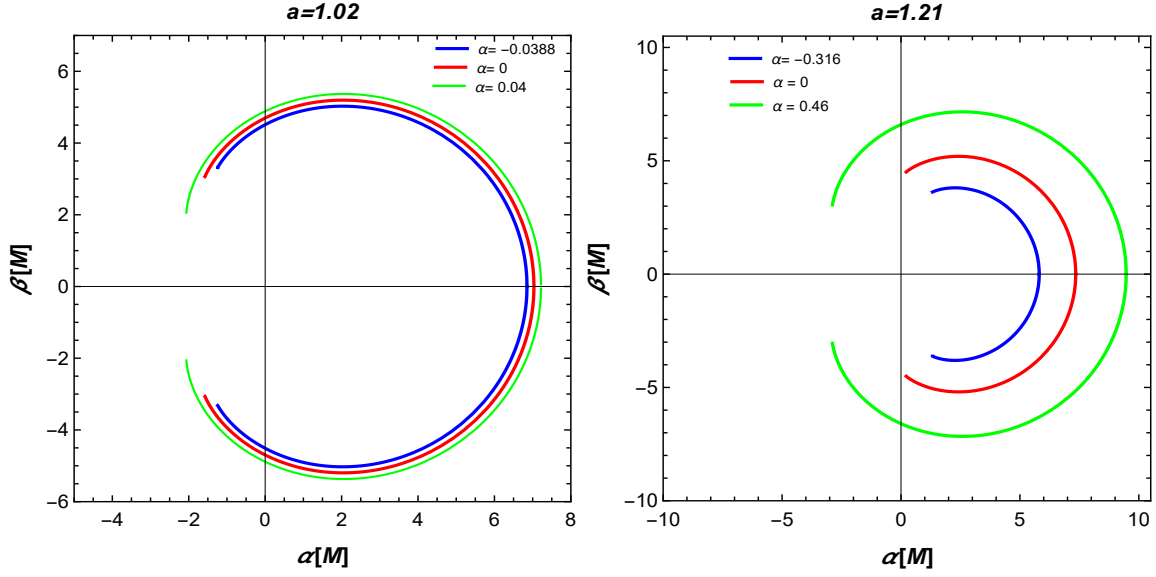
Figure 4.10. Shadows of a Kerr MOG naked singularity with observational inclinations angles "i", spin "a" and MOG parameter α. The plots from left to right are associated with i $= 90°$ and $\mathcal{M} = 1$. In the left plot, different colors correspond to different deformation parameter values with spin $a = 1.02$ and right with spin $a = 1.21$, according to the range of α.
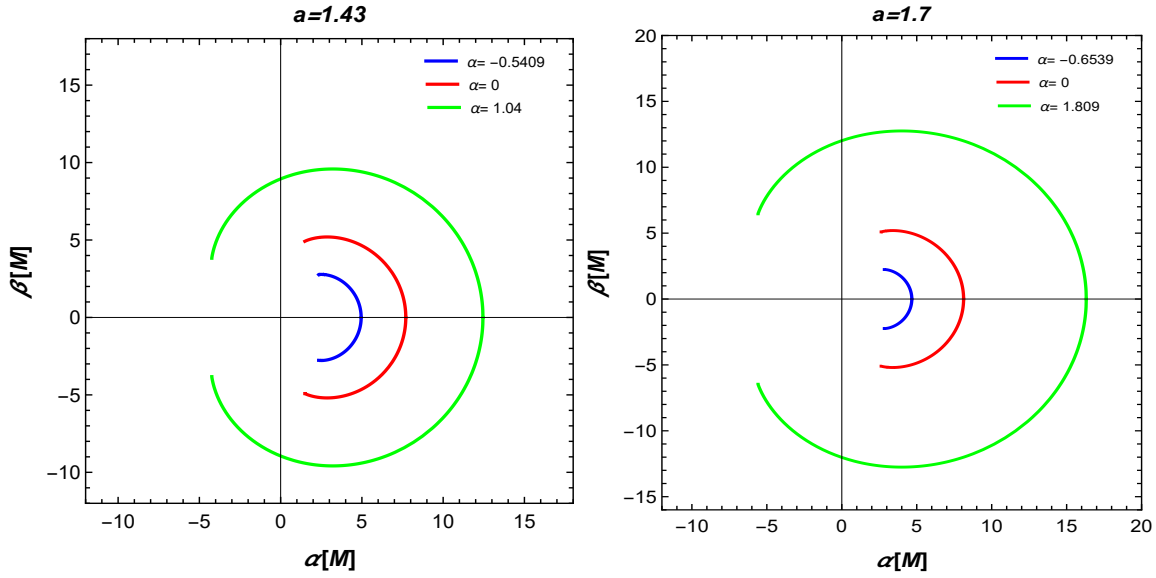
Figure 4.11. The plots from left to right are associated with i $= 90°$ and $\mathcal{M} = 1$. Different colors correspond to different deformation parameter values with spin $a = 1.43$ (left)and with spin $a = 1.7$ (right).

Figure 4.12. The plots from left to right are associated with i $= 90°$ and $M = 1$. In the left plot, different colors correspond to different deformation parameter values with spin $a = 1.95$ and right with spin $a = 2$.

In Fig. (4.12), we observe that for positive values of α, the radius of the photon sphere r_{ph}, increases.
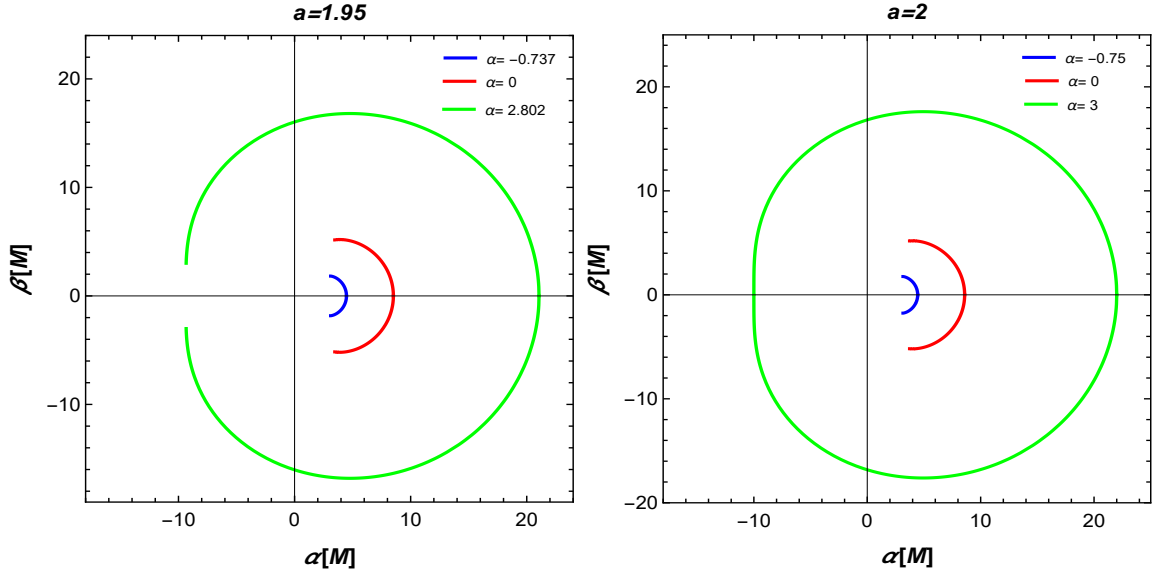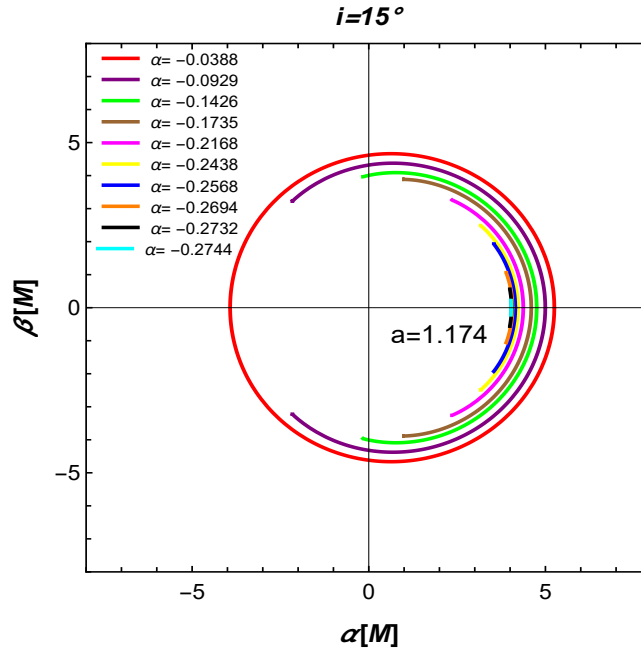

Figure 4.13. Shadows of Kerr MOG naked singularity with observational inclinations angles "i", spin "a" and MOG parameter α. The plot with different colors presents different spin values corresponding α, ranging from red indicating $a = 1$ to cyan representing the $a = 1.174$ for i $= 15°$ and $\mathcal{M} = 1$.
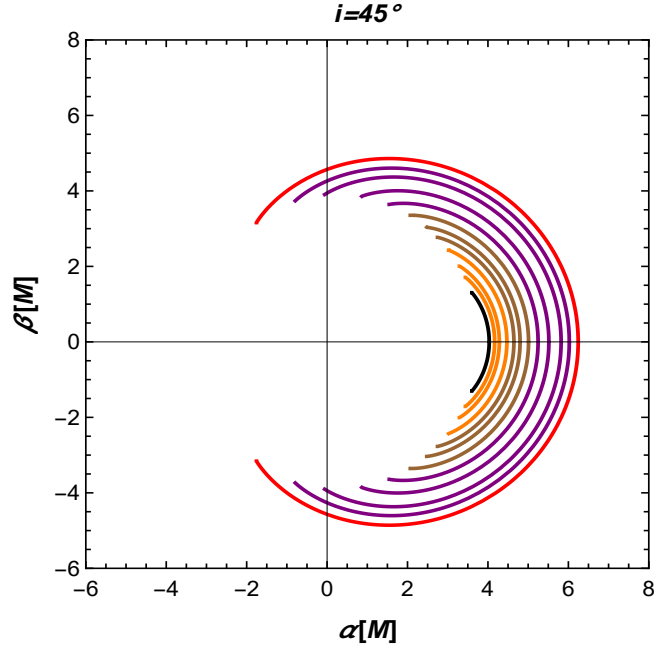
Figure 4.14. The plot with different colors presents different spin values corresponding α, ranging from red indicating $a = 1.02$ to black representing the $a = 1.52$ for $i = 45°$ and $\mathcal{M} = 1$.
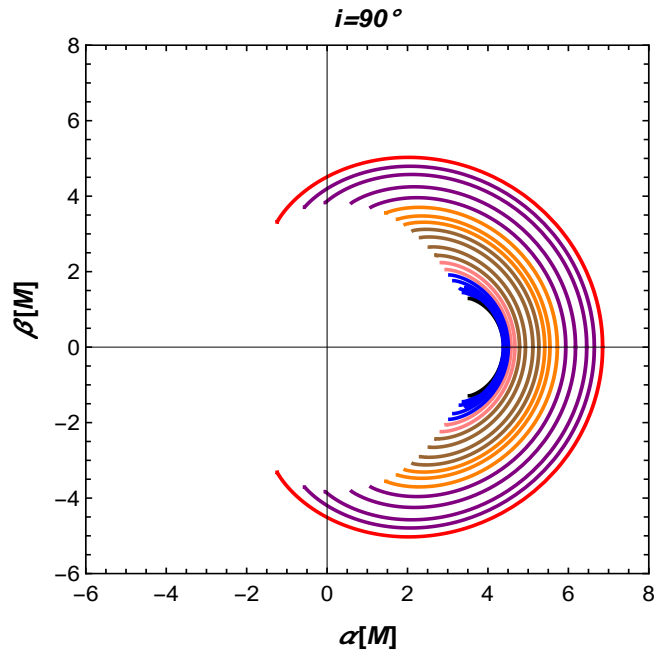
Figure 4.15. The plot with different colors presents different spin values corresponding α, ranging from red indicating $a = 1.02$ to black representing the $a = 2.5$ for $i = 90°$ and $\mathcal{M} = 1$.

This indicates a more complex arrangement of light orbits, possibly allowing for more stable photon trajectories. This results in a closed shadow, where light becomes confined

in a stable orbit around the singularity, forming a clearly defined boundary that can be observed.

The marginally stable orbit determines the closest stable circular orbit for matter. A reduction in r_{ms} implies that matter can maintain a stable orbit nearer to the singularity without being drawn into it. When we compute the $\zeta = 0$ and (4.42) numerically we find by changing the values of alpha with spin parameter r_{ms} decreases while r_{ph} increases and vice versa. This results in a scenario where the shadow takes on a closed form with gaps, as stable orbits contribute to the emergence of distinct light and dark regions within the shadow.In Fig. (4.13), it is illustrated that for lower inclination angles, such as i $= 15°$ (closer to face-on viewing), the gap in the shadow of a Kerr MOG naked singularity becomes noticeable at higher spin values and disappears at $a = 1.174m$ with MOG parameter α. In this figure, the shadow vanishes at a lower spinning value compared to that of the Kerr naked singularity in Fig. (2.5). This discrepancy arises due to the deformation parameter α.
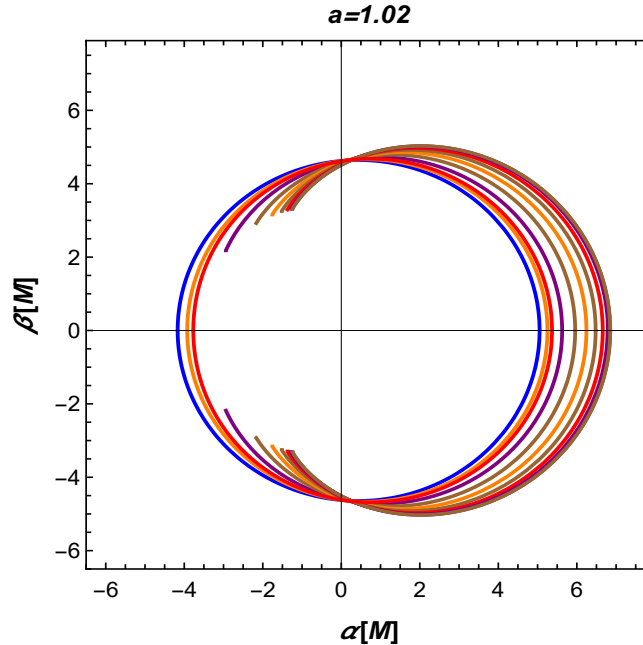
Figure 4.16. Shadows of Kerr MOG naked singularity with observational inclinations angles "i", spin "a" and MOG parameter α. The plot with different colors presents different inclination angles, ranging from blue indicating $i = 5°$ to brown representing the $i = 90°$ for $a = 1.02$ corresponding α and $\mathcal{M} = 1$.
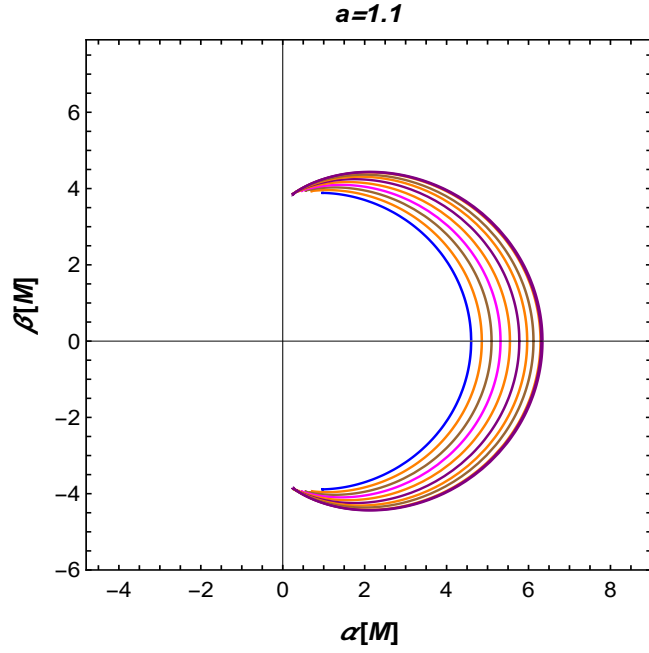
Figure 4.17. The plot with different colors presents different inclination angles, ranging from blue indicating $i = 5°$ to purple representing the $i = 90°$ for $a = 1.1$ corresponding α and $\mathcal{M} = 1$.
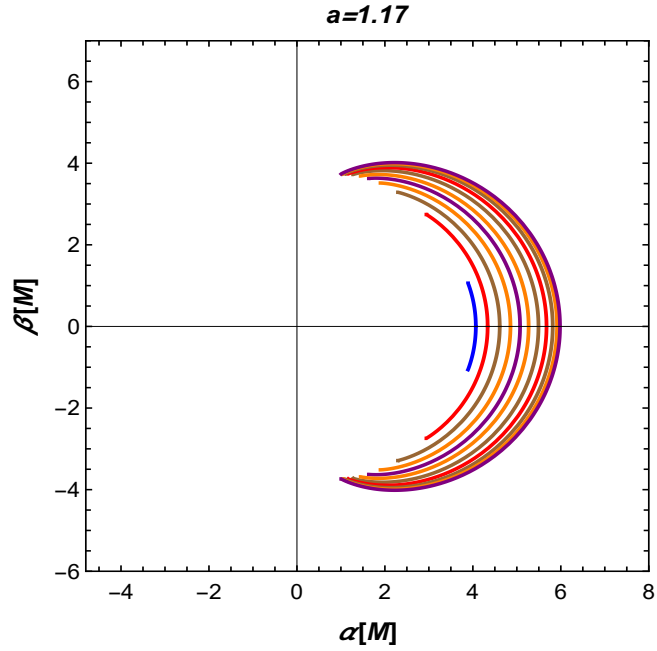
Figure 4.18. The plot with different colors presents different inclination angles, ranging from blue indicating $i = 5°$ to purple representing the $i = 90°$ for $a = 1.17$ corresponding α and $\mathcal{M} = 1$.

In Fig. (4.13), we observe that the shadow disappears at lower spins $a = 1.6$ as the inclination angle increases to i $= 45°$ due to the MOG parameter whereas, in Fig. (2.6), the

shadow does not vanish for Kerr naked singularity with this inclination angle. However, in Fig. (4.15), the shadow of the Kerr MOG naked singularity at a higher inclination angle does not disappear at lower spins, unlike what is observed in Figs. (4.12) and (4.13). In contrast, to Fig. (2.7), while the shadow does not vanish with this angle, its size does decrease with increasing spin. Furthermore, Figs. (4.16) and (4.17) show that a closed shadow can only occur with smaller inclination angles and spins within the range $1 < a \lesssim 1.1$. When $a \approx 1.1$, the shadow is open with a gap for all inclination angles, but for spins greater than $a \approx 1.1$, the shadow vanishes at smaller inclination angles.

So, a closed shadow forms when light rays become entirely confined by the gravitational pull of the singularity, resulting in a distinct and well-defined boundary that we can see in Figs. (4.13) and (4.16). The existence of a closed shadow indicates that the Kerr naked singularity possesses stable photon orbits, which is essential for differentiating it from black holes, as the latter usually feature event horizons that significantly affect the trajectories of light. The appearance of gaps within the shadow may signal the existence of incomplete photon spheres or unstable orbits. If gaps appear in the shadow, it suggests that some light paths are not captured, possibly due to the lack of a photon sphere or the presence of unstable orbits. This can produce observable features that distinguish it from black holes.

Chapter 5

Conclusion

This thesis probed how the shadow of a black hole is defined mainly by using its photon sphere with another intriguing feature, the shadow of naked singularity does not depend on the photon sphere. The shape and size of the black hole's shadow are determined by the mass of the black hole, its spin, and the observer's viewing angle. We further extended our understanding by analysis of the shadow which provides an initial way of figuring out the properties of the naked singularity. Furthermore, we explored the shadow of a Kerr black hole and naked singularity that appears in literature. Some characteristics associated with this comprise the fact that the shadow of a rotating black hole, like the Kerr black hole, exhibits shape deformation because of its spin parameter and vanishes as the distance of observers grows. On the other hand, the shadow shape of Kerr naked singularity depending on the range of spin $1 < a \lesssim 1.18$ [38], can be either closed or open.

The EHT group recently has successfully caught a polarized light around the M87* and Sgr A*. The orientation of light waves is apparent in these polarized images, and it is influenced by the magnetic field generated by the plasma revolving around the black holes. The results from these polarized images not only assure the presence of plasma around black holes but also give observations into the mechanisms that lead to their evolution and behavior [18]. Then, we focused on the shadow of a Kerr black hole under the influence of plasma and studied the light propagation through such a plasma medium. There are used

particular plasma distributions, which made the whole analysis analytically manageable. We computed an analytical formula following [34] outside the horizon of the Kerr black hole in the presence of plasma for the boundary curve of the shadow at any arbitrary point. We took into account homogeneous and inhomogeneous plasma distributions as depicted by figures in chapter 3.

In *chapter* 4 we observed the shadow casting by the Kerr MOG black hole in the presence of plasma and naked singularity. We discussed the inequalities [29] that establish the relationship of spin a and α, which distinguishes between Kerr MOG black hole and a naked singularity. The presence of plasma affects the trajectories of light rays within the domain of outer communication. The plasma possesses a frequency dependent refractive index, making it a dispersive medium. In a dispersive medium, photons with varying frequencies and wavelengths follow different trajectories. Here, we utilized the HJ equations and separated the equation by applying a specific condition on the plasma density and attained the generalized Carter constant. Based on the separability condition, we identify photon regions that meet this criterion and provide an analytical formula for the boundary curve of the shadow. The figures in this chapter present the intriguing behaviors of photon ring trajectories in both homogeneous and inhomogeneous media.

The observed facts indicate that deformations of shadow contour are different, compare them to the the distinct shadow structures for the Kerr black hole in the presence of plasma. By increasing the ratio $\frac{\omega_c^2}{\omega_0^2}$ expands the forbidden region until it entirely encloses the black hole at a critical value, $\frac{\omega_c^2}{\omega_0^2}$. At this point, the shadow vanishes for all observers, leading to a completely bright with $\frac{\omega_c^2}{\omega_0^2} \approx 17.45$ shadow vanishes. We also observed, the ratio $\frac{\omega_c^2}{\omega_0^2}$ depends on the metric model. However, in this case, it also varies with the MOG parameter α. As the values of spin parameter a are increased within the deformation parameter α, the ratio $\frac{\omega_c^2}{\omega_0^2}$ also increases.

Strong naked singularities, marked by pronounced deviations from black hole behavior, can generate shadows that are closed and display intricate structures, including multi-

ple rings or gaps. The presence of a closed shadow with unique characteristics poses a challenge to the cosmic censorship conjecture, which asserts that singularities must be concealed by event horizons. Observations of such shadows may offer evidence for the existence of strong naked singularities and their possible astrophysical consequences. Then we analyzed the shadow of Kerr MOG singularities and discussed the causal structure and some of the geometrical properties of naked singularities on Kerr MOG spacetime and the results are compared to those of Kerr naked singularities when deformation parameter $\alpha = 0$. We obtained some results by making comparisons with Kerr naked singularity. For lower inclination angles, such as i $= 15°$ (closer to face-on viewing), the gap in the shadow of a Kerr MOG naked singularity becomes noticeable at higher spin values and disappears at $a = 1.174$ with MOG parameter α and the shadow vanishes at a lower spinning value compared to that of the Kerr naked singularity. The shadow of the Kerr MOG naked singularity at a higher inclination angle does not disappear at lower spins, unlike what is observed for Kerr naked singularity for which the shadow does not vanish with this angle, its size does decrease with increasing spin. Furthermore, we find from the figures that a closed shadow can only occur with smaller inclination angles and spins within the range $1 < a \lesssim 1.1$. When $a \approx 1.1$, the shadow is open with a gap for all inclination angles, but for spins greater than $a \approx 1.1$, the shadow vanishes at smaller inclination angles. This discrepancy arises from α deformation parameter, allowing us to make our results comparable.

Bibliography

[1] S. Schaffer, "John Michell and Black Holes," *Journal for the History of Astronomy*, vol. 10, 42(1979).

[2] J. Gribbin, *Einstein's Masterwork: 1915 and the General Theory of Relativity*. Icon Books Ltd, (2015).

[3] L. P. Hughston and K. P. Tod, *An Introduction to General Relativity*. Cambridge University Press, (1990).

[4] S. Carlip, "Black Hole Thermodynamics," *International Journal of Modern Physics D*, vol. 23, 1430023(2014).

[5] S. M. Carroll, *Spacetime and Geometry*. Cambridge University Press, (2019).

[6] K. Schwarzschild, "On the Gravitational Field of a Mass Point According to Einstein's Theory," *Sitzungsberichte der königlich preussischen Akademie der Wissenschaften*, 189(1916).

[7] R. P. Kerr, "Gravitational Field of a Spinning Mass as an Example of Algebraically Special Metrics," *Physical review letters*, vol. 11, 237(1963).

[8] J. A. Wheeler, "Our Universe: The Known and the Unknown," *The American Scholar*, 248(1968).

[9] D. R. Wilkins, L. Gallo, E. Constantini., *et al.*, "Light Bending and X-ray Echoes from behind a Supermassive Black Hole," *The Astrophysical Journal*, 22(2021).

[10] J.-P. Luminet, "An Illustrated History of Black Hole Imaging," *arXiv preprint arXiv:1902.11196*, (2019).

[11] M. De Laurentis and P. Salucci, "The Accurate Mass Distribution of M87*, the Giant Galaxy with Imaged Shadow of its Supermassive Black Hole, as a Portal to New Physics," *The Astrophysical Journal*, vol. 929, 17(2022).

[12] G. Weinstein, "Why Do You Think it is a Black Hole?," *arXiv:2102.02592*, (2021).

[13] M. Honma, "Imaging the Supermassive Black Hole at the Center of the Milky Way Galaxy," *JSAP Review*, vol. 2023, p. 230213, 230213(2023).

[14] R. Kumar and S. G. Ghosh, "Black Hole Parameter Estimation from Its Shadow," *Springer Nature*, vol. 892, 78(2020).

[15] J. L. Synge, "The Escape of Photons from Gravitationally Intense Stars," *Monthly Notices of the Royal Astronomical Society*, vol. 131, 463(1966).

[16] J. L. Synge, "Equations of Motion in General Relativity," in *Proceedings of the Royal Irish Academy. Section A: Mathematical and Physical Sciences*, JSTOR, 38(1970).

[17] H. Falcke, F. Melia, and E. Agol, "Viewing the Shadow of the Black Hole at the Galactic Center," *The Astrophysical Journal*, vol. 528, 13(1999).

[18] K. Akiyama, A. Alberdi, W. Alef, J. C. Algaba, *et al.*, "First Sagittarius A* Event Horizon Telescope Results. VII. Polarization of the Ring," *The Astrophysical Journal Letters*, vol. 964, 25(2024).

[19] M. Wang, S. Chen, and J. Jing, "Chaotic Shadows of Black Holes: a Short Review," *Communications in Theoretical Physics*, vol. 74, p. 097401, 097401(2022).

[20] E. Teo, "Spherical Orbits around a Kerr Black Hole," *General Relativity and Gravitation*, vol. 53, 10(2021).

[21] R. Penrose, "Gravitational Collapse and Space-Time Singularities," *Physical Review Letters*, vol. 14, 57(1965).

[22] D. Patel, V.and Tahelyani, A. B. Joshi, D. Dey, and P. S. Joshi, "Light Trajectory and Shadow Shape in the Rotating Naked Singularity," *The European Physical Journal C*, vol. 82, 798(2022).

[23] S. J. Pankaj, "Equilibrium Configurations from Gravitational Collapse," *Classical and Quantum Gravity*, (2011).

[24] K. Akiyama, A. Alberdi, *et al.*, "First M87* Event Horizon Telescope Results. i. The Shadow of the Supermassive Black Hole," *The Astrophysical Journal Letters*, vol. 875, 6(2019).

[25] K. Akiyama, A. Alberdi, *et al.*, "First Sagittarius A* Event Horizon Telescope Results. i. The Shadow of the Supermassive Black Hole in the Center of the Milky Way," *The Astrophysical Journal Letters*, vol. 930, 12(2022).

[26] A. B. Joshi, D. Dey, P. S. Joshi, and P. Bambhaniya, "Shadow of a Naked Singularity without Photon Sphere," *Physical Review D*, vol. 102, p. 024022, 024022(2020).

[27] A. I. Janis, E. T. Newman, and J. Winicour, "Reality of the schwarzschild singularity," *Physical Review Letters*, vol. 20, 878(1968).

[28] P. Sheoran, A. Herrera-Aguilar, and U. Nucamendi, "Mass and Spin of a Kerr Black Hole in Modified Gravity and a Test of the Kerr Black Hole Hypothesis," *Physical Review D*, vol. 97, 124049(2018).

[29] P. Pradhan, "Distinguishing Black Hole and Naked Singularity in MOG via Inertial Frame Dragging Effect," *arXiv preprint arXiv:2007.01347*, (2020).

[30] J. W. Moffat, "Scalar Tensor Vector Gravity Theory," *Journal of Cosmology and Astroparticle Physics*, 004(2006).

[31] X. M. Deng, Y. Xie, and T. Y. Huang, "Modified Scalar-Tensor-Vector Gravity Theory and the Constraint on Its Parameters," *Physical Review D—Particles, Fields, Gravitation, and Cosmology*, vol. 79, 044014(2009).

[32] D. Muhleman and I. Johnston, "Radio Propagation in the Solar Gravitational Field," *Physical Review Letters*, vol. 17, 455(1966).

[33] R. A. Breuer and J. Ehlers, "Propagation of High-Frequency Electromagnetic Waves through a Magnetized Plasma in Curved Space-time. I," *Proceedings of the Royal Society of London. A. Mathematical and Physical Sciences*, vol. 370, 389(1980).

[34] V. Perlick and O. Y. Tsupko, "Light Propagation in Plasma on Kerr Spacetime: Separation of the Hamilton-Jacobi Equation and Calculation of the Shadow," *Physical Review D*, vol. 95, 104003(2017).

[35] M. Visser, "The Kerr Spacetime: A Brief Introduction," *arXiv preprint arXiv:0706.0622*, (2007).

[36] V. Perlick and O. Y. Tsupko, "Calculating Black Hole Shadows: Review of Analytical Studies," *Physics Reports*, vol. 947, 39(2022).

[37] B. Houchmandzadeh, "The Hamilton–Jacobi Equation: An Alternative approach," *American Journal of Physics*, vol. 88, pp. 353–359, 353(2020).

[38] B. Nguyen, P. Christian, and C.-K. Chan, "Shadow Geometry of Kerr Naked Singularities," *The Astrophysical Journal*, vol. 954, 78(2023).

[39] P. Volker, "Gravitational lensing from a Spacetime Perspective," *Living reviews in relativity*, (2004).

[40] M. D. Johnson, A. Lupsasca, *et al.*, "Universal Interferometric Signatures of a Black Hole's Photon Ring," *Science Advances*, vol. 6, eaaz1310(2020).

[41] D. Charbulák and Z. Stuchlík, "Spherical Photon Orbits in the Field of Kerr Naked Singularities," *The European Physical Journal C*, vol. 78, 78(2018).

[42] V. Perlick, *Ray Optics, Fermat's Principle, and Applications to General Relativity.* Springer Science & Business Media, (2000).

[43] S. Liu, "Electromagnetic Fields, Size, and Copy of a Single Photon," *arXiv:1604.03869*, 2016.

[44] A. Grenzebach, V. Perlick, and C. Lämmerzahl, "Photon Regions and Shadows of Kerr-Newman-NUT Black Holes with a Cosmological Constant," *Physical Review D*, vol. 89, 124004(2014).

[45] J. Bardeen, "Black Holes ed C. DeWitt and BS DeWitt," (1973).

[46] V. Perlick, O. Y. Tsupko, and G. S. Bisnovatyi-Kogan, "Influence of a Plasma on the Shadow of a Spherically Symmetric Black Hole," *Physical Review D*, vol. 92, 104031(2015).

[47] S. L. Corre, "Dark Matter, a New Proof of the Predictive Power of General Relativity," *arXiv preprint arXiv:1503.07440*, (2015).

[48] P. D. Mannheim, "Alternatives to Dark Matter and Dark Energy," *Progress in Particle and Nuclear Physics*, vol. 56, 340(2006).

[49] S. Tsujikawa, "Modified Gravity Models of Dark Energy," in *Lectures on cosmology: Accelerated Expansion of the Universe*, Springer, 99(2010).

[50] S. R. Chowdhury and M. Khlopov, "Gravitational Waves in the Modified Gravity," *arXiv preprint arXiv:2111.07704*, (2021).

[51] J. Moffat, "Modified Gravity Black Holes and their Observable Shadows," *The European Physical Journal C*, vol. 75, 130(2015).

[52] G. Briozzo and E. Gallo, "Analytical Expressions for Pulse Profile of Neutron Stars in Plasma Environments," *The European Physical Journal C*, vol. 83, 165(2023).

[53] H. Wang, Y. M. Xu, and S. W. Wei, "Shadows of Kerr-like Black Holes in a Modified Gravity Theory," *Journal of Cosmology and Astroparticle Physics*, vol. 2019, 046(2019).